Geochemistry Geophysics Geosystems G3
AN ELECTRONIC JOURNAL OF THE EARTH SCIENCES
Published by AGU and the Geochemical Society

*Article*
Volume 3, Number 11
22 November 2002
8503, doi:10.1029/2002GC000334
ISSN: 1525-2027

# Motion of the Easter hot spot relative to Hawaii and Louisville hot spots

**Bernhard Steinberger**
*Cooperative Institute for Research in Environmental Sciences, University of Colorado, Boulder, Colorado 80309, USA (bernhars@cires.colorado.edu)*

[1] Hot spots have been widely used as a fixed reference frame for plate motions; however, it should be expected that the underlying plumes are advected in a dynamic mantle. Here a simple numerical model of hot spot motion due to large-scale mantle flow is applied to the Easter, Hawaii and Louisville hot spots. Computations are performed for a range of different buoyant plume rising speeds, ages and locations, mantle density and viscosity structures, etc. It is shown that a westward motion of the Easter hot spot at several cm per year relative to Hawaii and Louisville hot spots is a robust result for a large range of model parameters. In order to obtain an appropriate boundary condition for mantle flow near the Easter hot spot and to find out on which plate to expect the Easter hot spot track for a given time, published isochrons were rotated to the past ridge locations in a reference frame that takes the computed motion of Hawaii and Louisville hot spots into account. Calculations that include flow in the mantle and therefore relative movement of hot spots yield a better explanation of the observed age distribution along the Sala y Gomez ridge than assuming hot spot fixity; at the same time they predict a hot spot track on the Nazca plate that is roughly similar to the shape of the Nazca and Sala y Gomez ridges. Furthermore, the Easter hot spot was in an intraplate location on the Nazca plate during the past 43 Ma, somewhat closer to the ridge between ~43 and 26 Ma than between ~26 Ma and now. In contrast, if hot spots are assumed fixed, a location close to the ridge and rather on the Pacific plate between ~43 and 26 Ma is predicted. Based on morphology and gravity signature it is suggested that the Nazca ridge and the eastern Tuamotu Island Plateau were created by plume material that erupted at the East Pacific Rise while the Easter plume was located sufficiently close to enable such an interaction, whereas the Sala y Gomez ridge was formed above the Easter plume in an intraplate setting. This implies that, if hot spots have indeed moved as computed here, during formation of the Nazca ridge (between ~43 and 26 Ma) plume material erupted at the ridge several 100 km away from the plume, whereas no volcanism occurred directly above the plume. It also implies that any seamounts on the Pacific plate east of the Tuamotu Plateau are unrelated to the Easter plume.

**Components:** 12,381 words, 14 figures, 1 table.

**Keywords:** Mantle plume; mantle flow; hot spot track; Nazca plate; isochrons; tomography.

**Index Terms:** 3040 Marine Geology and Geophysics: Plate tectonics (8150, 8155, 8157, 8158); 3210 Mathematical Geophysics: Modeling; 8121 Tectonophysics: Dynamics, convection currents and mantle plumes; 9355 Information Related to Geographic Region: Pacific Ocean.

**Received** 23 May 2001; **Revised** 8 July 2001; **Accepted** 16 July 2002; **Published** 22 November 2002.

Steinberger, B., Motion of the Easter hot spot relative to Hawaii and Louisville hot spots, *Geochem. Geophys. Geosyst.*, *3*(11), 8503, doi:10.1029/2002GC000334, 2002.

**Theme:** Plume-Ridge Interaction **Guest Editor:** David Graham

# 1. Introduction

## 1.1. Question of Hot Spot Fixity

[2] The question as to what degrees hot spots – regions of intraplate volcanism, such as Hawaii, or especially intensive volcanism along mid-ocean ridges, such as Iceland – are fixed relative to each other has received considerable attention recently. The fixity of Pacific hot spots relative to hot spots on other plates has been at the center of this debate. *Morgan* [1972] proposed that island and seamount chains in the Pacific have formed as the Pacific plate moved over a set of hot spots that are fixed and hence can be used as a reference frame for plate motions. The most widely accepted explanation for these hot spots is that they are formed by narrow convective upwellings, so-called plumes [*Morgan*, 1972] from deep inside the mantle, presumably from the thermal boundary at the base of the mantle. These plume conduits are believed to be established trailing large plume heads [*Richards et al.*, 1989]. The conduits, however, rise through a convecting mantle, and should therefore be expected to be advected and tilted over time, and the "hot spots", where they reach the surface, should move accordingly. It has also been known that plate circuit reconstructions combined with assuming Hawaiian hot spot fixity relative to African hot spots yield a predicted Hawaiian hot spot track incompatible with what is observed, particularly prior to 43 Ma [*Molnar and Stock*, 1987].

[3] One of the largest uncertainties of these plate circuits had been the motion between East and West Antarctica, but new results [*Cande et al.*, 2000] have put firmer constraints on this. Also, paleolatitude data from the Emperor Chain indicate a latitude of the Hawaiian hot spot during the Cretaceous farther north than at present [*Tarduno and Cottrell*, 1997; *Tarduno et al.*, 2001]. Both observations have been interpreted in terms of a rapid southward motion of the Hawaiian hot spot, especially prior to 43 Ma. Numerical calculations of flow in the mantle [*Steinberger and O'Connell*, 2000] have predicted a southeastward motion of the Hawaiian hot spot in the mean mantle (no-net-rotation) reference frame of these calculations. The results are compatible with the relative fixity of hot spots on the Pacific plate, because they tend to predict a similar motion towards the east or southeast for all hot spots on the Pacific plate, and a small relative motion among them.

## 1.2. Importance of the Easter Hot Spot in Assessing Hot Spot Fixity

[4] For a hot spot located around Easter Island, however, these flow calculations predict a motion in a different direction, and the predicted motion relative to hot spots on the Pacific plate is up to a few cm per year. This result can be qualitatively understood: whereas in the low-viscosity upper mantle the motion of the conduit is dominated by buoyant rising, in the high-viscosity lower mantle it is strongly advected laterally. Therefore the surface motion mostly represents flow in the upper part of the lower mantle [*Steinberger and O'Connell*, 2000]. The flow at that depth tends to be opposite to plate motions under both Nazca and Pacific plates, i.e., towards spreading ridges.

[5] The relative motion between the Nazca plate, on which the Easter hot spot is located, and the Pacific plate is rather well constrained for times for which magnetic isochrons are identified on both plates, because no intervening plate circuits are required. It should therefore be relatively easy to compare radiometric ages and the geometry of hot spot tracks to predictions based on either mantle flow computations, or assuming hot spot fixity. Thus the Easter hot spot offers an excellent test of hot spot fixity. The results presented by *Steinberger and O'Connell* [2000] show that computations of hot spot motion based on mantle flow can in fact explain the (scarce) measured ages along the tracks better than the assumption of hot spot fixity, but discrepancies between predicted and observed hot spot track remain.

[6] Another important aspect of the Easter hot spot is its close proximity to the East Pacific Rise. Changes in ridge geometry and associated changes in mantle flow should therefore cause a motion of the hot spot. By comparing computed and actual hot spot tracks we gain additional information

about the past ridge geometry, as well as the interaction of plume and mantle flow.

### 1.3. Outline of Approach Pursued Here

[7] Because of the central position of the Easter hot spot in Pacific hot spot motion [*Steinberger and O'Connell*, 1998], a more detailed discussion is presented here. First, a larger number of calculations of hot spot motion for different mantle density and viscosity structures, different buoyant plume rising speeds, ages and locations, different plate boundary locations etc. are shown, thus showing the dependence of results on various assumptions, and the robustness of the previously computed motion of the Easter hot spot relative to Hawaii and Louisville hot spots. Furthermore, an improved representation of the mantle flow field is used: Because of the proximity of the Easter hot spot to a plate boundary, it is desirable to construct the plate boundary location as a function of time as accurately as possible, in order to obtain a suitable kinematic flow field (i.e., the part of the flow field that is related to plate motions, following *Hager and O'Connell* [1979, 1981]). An accurate reconstruction of the plate boundary is also needed to determine on which plate the hot spot was located through time, hence on which plate a hot spot track can be expected. Here a plate boundary evolution that is consistent with magnetic lineations and represents both continuous ridge migration and ridge jumps is used. The kinematic flow field is expanded up to spherical harmonic degree 255, thus giving a better resolved estimate of mantle flow close to a plate boundary. Previously, we used an expansion up to degree 31.

[8] An important aspect of this particular hot spot is the fact that there is no clear age progression of volcanism around Easter Island. Rather there appears to be simultaneous recent volcanism over an area of several hundred km East-West extent (D. Naar, unpublished data). It has thus been proposed that volcanism near Easter Island is not caused by a plume at all, rather a "mantle hot line" [*Bonatti et al.*, 1977]. However, evidence for the existence of mantle plumes is, besides observations [*Morgan*, 1972; *Richards et al.*, 1989] given by numerous experiments and theoretical results [e.g., *Whitehead and Luther*, 1975; *Olson and Singer*, 1985; *Griffiths and Campbell*, 1990], whereas there is no such experimental support for "mantle hot lines". Therefore, it is assumed here that the Easter Island region is indeed underlain by a mantle plume and that the large extent of simultaneous volcanism is due to plume-ridge interaction, i.e. westward channeling of plume material toward the East Pacific Rise and eruption of magmas through thin lithosphere [*Schilling*, 1991; *Kingsley and Schilling*, 1998]. Because recent volcanism is widespread, different locations for an Easter hot spot plume have been proposed: *Hanan and Schilling* [1989] propose a hot spot location close to Sala y Gomez Island, based on an empirical curve of "waist-width" of plume-affected ridge versus plume-ridge distance. Also, *O'Connor et al.* [1995], *Pan and Batiza* [1998] and *Kingsley and Schilling* [1998] favor a location close to Sala y Gomez Island (−26.5°S, −105.5°W), however *Haase et al.* [1996] argue for a location near Easter Island (27.1°S, −109.3°W). Due to the conflicting evidence, I will, in most cases, assume a plume location half-way between Easter and Sala y Gomez islands, but plume locations at either island will also be considered.

[9] The approach used here consists of the following steps: In section 2, the motion of Hawaiian and Louisville hot spot due to large-scale mantle flow is computed for a number of different cases, using essentially the same modeling approach as described by *Steinberger and O'Connell* [1998, 2000] and *Steinberger* [2000]. In the next step, the Pacific plate motion is re-computed under consideration of Hawaiian and Louisville hot spot motion, and compared to the Pacific plate motion computed under the assumption that these hot spots are fixed. Hawaii and Louisville are the only two hot spots on the Pacific plate associated with tracks that span the period between 43 Ma and present and show a clear age progression, hence only these two hot spots are used to determine Pacific plate motions. Relative plate motions are not modified in this step, so the absolute motion of other plates (e.g., the Nazca plate) is also changed. The inferred

past location of the boundary between the Pacific and Nazca plates also depends on the plate motions; how the boundary is constructed is hence shown in section 3.

[10] In section 4, the computed plate motions and boundaries are used to compute the motion of the Easter hot spot and its hot spot track on the Nazca plate. The geometry and age progression of the computed hot spot track are then compared to observations. Obviously, changing plate boundaries also has an effect on the computed Hawaiian and Louisville hot spot motions. It turns however out that the effect on the motion of these two hot spots is rather minor during the past 43 Ma, therefore an iteration of re-computing hot spot motion, plate motion, and so on, is not carried out. Finally, although the computations can not exactly reproduce the inflection between Sala y Gomez and Nazca ridges, they suggest an explanation for it. A discussion about this feature, and a suggested scenario of the overall tectonic evolution of the region that could qualitatively explain this feature, is given in section 5.

[11] For the computation of mantle flow, on which this whole approach is based, surface plate motions in a "no-net-rotation" reference frame are used as boundary conditions. Because no lateral viscosity variations are considered, a net rotation of the lithosphere relative to the underlying mantle cannot occur in the computation. Hence mantle flow, and, in the following steps, hot spot motions, plate motions and plate boundaries are computed in the same reference frame. For the real Earth though, such a net rotation can occur, due to lateral viscosity variations in the lithosphere [*O'Connell et al.*, 1991], therefore this reference frame does not necessarily correspond to the actual lithospheric no-net-rotation reference frame, and is not directly tied to any observations. While this "mantle reference frame" as it will be called in the following, is thus a somewhat abstract concept, it should also be noted that the computed Easter hot spot track on the Nazca plate, which is, in the final step, compared to observations, depends essentially on the motion of the Easter hot spot relative to Hawaii and Louisville hot spots. Hence the mantle reference frame is not important for the main conclusions of this work. For a more detailed discussion of reference frames see also *Steinberger and O'Connell* [1998].

## 2. Computations of Hawaii and Louisville Hot Spot Motion and Absolute Pacific Plate Motion

[12] The calculation of hot spot motion consists essentially of two steps: In a first step, a time-dependent large-scale mantle flow field is computed [*Hager and O'Connell*, 1979, 1981] based on surface plate motions [*Lithgow-Bertelloni et al.*, 1993; *Gordon and Jurdy*, 1986] and, in most cases, internal density heterogeneities. The latter are inferred here from seismic tomography models. In a second step, the motion of a plume conduit, that moves with this large-scale flow, but also rises buoyantly, and hence the motion also of the hot spot at the top of this conduit is computed. This plume model was suggested by *Richards and Griffiths* [1988]. Details of the computation are described elsewhere [*Steinberger and O'Connell*, 1998] and are not repeated here.

[13] The model assumptions (such as viscosity structures, relation between seismic velocity and density anomalies, buoyant plume rising speed etc.) contain a certain degree of uncertainty. They have been described and justified in detail in previous work [*Steinberger and O'Connell*, 1998, 2000; *Steinberger*, 2000]. Here I assume that the source of the Louisville hot spot has been active since 120 Ma, the age of the Ontong-Java plateau, proposed to have been formed by the Louisville plumehead [*Richards et al.*, 1989]. Since the beginning of the Hawaiian-Emperor chain has been subducted, its age is unknown. In most calculations, I will also assume a start-up "age" of 120 Ma. This means that the computations are initialized with vertical conduits 120 Ma ago. This initial condition is based on the assumption that plume conduits are established by fast-rising plume heads [*Richards et al.*, 1989], and hence initially are vertical. In most cases, the computed Hawaiian hot spot motion depends only moderately on the assumed hot spot age, e.g. assuming

**Table 1.** Rotation Rates of the Pacific Plate in Either a Fixed Hot Spot Reference Frame (First Three Cases) or Mantle Reference Frame (All Other Cases)[a]

| # | TM | SF | MVM | $u_0$ | PVM | td | adv | com | 670 | lat1 | long1 | mag1 | lat2a | long2a | mag2a | lat2b | long2b | mag2b |
|---|---|---|---|---|---|---|---|---|---|---|---|---|---|---|---|---|---|---|
| 1 | | | | | | | | | | −67.33 | 118.17 | 0.7688 | −70.60 | 109.11 | 0.9216 | −59.70 | 131.62 | 0.5562 |
| 2 | | | | | | | | | | −69.00 | 112.00 | 0.7670 | | | | | | |
| 3 | | | | | | | | | | −68.00 | 105.00 | 0.8095 | | | | | | |
| 4 | 1 | 1 | II | 0.86 | 1 | y | y | n | nb | −72.00 | 126.78 | 0.6867 | −76.28 | 102.11 | 0.8272 | −59.42 | 157.01 | 0.5083 |
| 5 | 1 | 3 | II | 0.86 | 1 | y | y | n | nb | −72.61 | 144.01 | 0.6175 | −77.25 | 102.11 | 0.8064 | −49.96 | −171.74 | 0.4151 |
| 6 | 1 | 1 | III | 0.86 | 1 | y | y | n | nb | −71.25 | 122.10 | 0.6608 | −76.34 | 95.90 | 0.8168 | −54.61 | 151.17 | 0.4659 |
| 7 | 5 | 1 | II | 0.86 | 1 | y | y | n | nb | −66.70 | 133.40 | 0.7356 | −70.56 | 128.25 | 0.8465 | −59.36 | 142.58 | 0.5707 |
| 8 | 5 | 1 | I | 2.00 | 1 | y | y | n | nb | −66.78 | 136.94 | 0.7443 | −70.70 | 130.94 | 0.8570 | −59.41 | 147.48 | 0.5777 |
| 9 | 5 | 1 | III | 0.86 | 1 | y | y | n | nb | −66.84 | 133.09 | 0.7460 | −70.55 | 128.32 | 0.8610 | −59.76 | 141.78 | 0.5745 |
| 10 | 5 | 2 | III | 0.86 | 1 | y | y | n | nb | −67.66 | 136.53 | 0.7329 | −71.67 | 131.95 | 0.8430 | −59.91 | 144.96 | 0.5702 |
| 11 | 4 | 1 | II | 0.86 | 1 | y | y | n | nb | −69.68 | 115.95 | 0.7094 | −72.31 | 109.41 | 0.8311 | −64.22 | 125.85 | 0.5261 |
| 12 | 4 | 1 | I | 2.00 | 1 | y | y | n | nb | −70.66 | 119.08 | 0.6910 | −73.15 | 111.81 | 0.7895 | −65.99 | 129.90 | 0.5433 |
| 13 | 4 | 1 | III | 0.86 | 1 | y | y | n | nb | −70.96 | 110.87 | 0.7076 | −73.35 | 103.73 | 0.8287 | −65.79 | 121.21 | 0.5256 |
| 14 | 3 | 1 | II | 0.86 | 1 | y | y | n | nb | −72.21 | 160.92 | 0.7446 | −77.56 | 176.92 | 0.8621 | −57.42 | 151.90 | 0.5952 |
| 15 | 3 | 1 | III | 0.86 | 1 | y | y | n | nb | −73.41 | 174.82 | 0.7110 | −75.75 | −133.75 | 0.8367 | −46.53 | 145.85 | 0.6520 |
| 16 | 2 | 1 | II | 0.86 | 1 | y | y | n | nb | −67.20 | 121.70 | 0.7662 | −70.43 | 111.93 | 0.8815 | −61.16 | 136.81 | 0.5984 |
| 17 | 2 | 1 | I | 2.00 | 1 | y | y | n | nb | −66.78 | 118.64 | 0.7944 | −69.44 | 112.97 | 0.9025 | −61.90 | 127.19 | 0.6305 |
| 18 | 2 | 1 | III | 0.86 | 1 | y | y | n | nb | −66.61 | 119.34 | 0.7794 | −69.26 | 110.58 | 0.8971 | −61.88 | 133.21 | 0.6052 |
| 19 | | | II | 0.86 | 1 | y | | n | cb | −63.33 | 132.78 | 0.7070 | −70.23 | 124.35 | 0.8384 | −48.09 | 146.63 | 0.5376 |
| 20 | | | I | 2.00 | 1 | y | | n | cb | −63.15 | 136.92 | 0.7284 | −70.22 | 127.67 | 0.8605 | −48.05 | 151.69 | 0.5606 |
| 21 | | | III | 0.86 | 1 | y | | n | cb | −63.03 | 133.78 | 0.7126 | −70.05 | 126.38 | 0.8417 | −47.85 | 146.38 | 0.5464 |
| 22 | 4 | 1 | III | 2.38 | 2 | y | y | n | nb | −70.99 | 111.99 | 0.6860 | −74.17 | 111.97 | 0.7825 | −63.45 | 111.92 | 0.5394 |
| 23 | 4 | 1 | III | 0.86 | 1 | y | n | n | nb | −69.66 | 130.27 | 0.7111 | −73.37 | 124.59 | 0.8054 | −62.74 | 139.17 | 0.5736 |
| 24 | 4 | 1 | III | 0.86 | 1 | n | n | n | nb | −65.99 | 119.04 | 0.6438 | −71.92 | 123.02 | 0.7232 | −52.31 | 117.67 | 0.5433 |
| 25 | 4 | 1 | III | 0.86 | 1 | y | y | n | pb | −71.13 | 109.46 | 0.7075 | −73.74 | 100.80 | 0.8272 | −65.35 | 122.19 | 0.5306 |
| 26 | 4 | 1 | III | 0.86 | 1 | y | y | y | nb | −69.35 | 110.69 | 0.7311 | −72.34 | 100.73 | 0.8697 | −62.44 | 126.24 | 0.5306 |

[a] Case 1 was computed with the same method as the cases with moving hot spots. Cases 2 and 3 were previously published [*Gordon and Jurdy*, 1986; *Duncan and Clague*, 1985]. Other cases are for computed hot spot motions, as described in the text. The columns indicate: TM, Tomography model; 1, S12WM13 [*Su et al.*, 1994]; 2, SAW24B16 [*Megnin and Romanowicz*, 2000]; 3, SB4L18 [*Masters et al.*, 2000]; 4, S2ORTS *Ritsema and Van Heijst* [2000]; 5, S. Grand's model, obtained in January 2001 (ftp://bratsche.geo.utexas.edu/outgoing/steveg), a further development of *Grand* [1994] and *Grand et al.* [1997]; SF, scaling factors $(\delta\rho/\rho)/(\delta\upsilon_s/\upsilon_s)$ to convert seismic velocity to density variations: 1, Scaling factor 0.2; only mantle density anomalies below 220 km depth are included; 2, Scaling factor 0.3, only mantle density anomalies below 220 km depth are included; 3, Scaling factor 0.2, all mantle density anomalies are included. MVM, mantle viscosity structure (see Figure 1). $u_0$, conduit rising speed for a plume with anomalous mass flux $B_0 = 10^3$ kg/s and surrounding mantle viscosity of $\eta_0 = 10^{21}$ Pas in units of cm/yr. PVM, plume viscosity model (specifies whether equation 1 or 2 are used to compute conduit rising speed). td, time-dependent plate motion boundary condition (yes/no). adv, advection of density heterogeneities (yes/no). com, compressible mantle (yes/no). 670 = treatment of 410 km and 670 km boundary. nb, no boundary to flow assumed; pb, phase boundaries assumed, same phase boundary parameters as in *Steinberger* [2000]; cb, chemical boundary (i.e., layered mantle flow) at 670 km, no boundary at 410 km assumed. lat1, long1, rate1, latitude and longitude (degrees) and magnitude (degrees/Myr) of best fitting constant plate rotation rate 0–43 Ma. lat2a, long2a, rate2a and lat2b, long2b, rate2b, latitude and longitude (degrees) and magnitude (degrees/Myr) of best fitting plate rotation rates 0–25 and 25–43 Ma, allowing for two constant rotation rates. In all cases, an age 120 Ma is assumed for both Hawaii and Louisville hot spot, except for cases 14 and 15, where an age 100 Ma is assumed for Hawaii. Flow fields in cases 19–21 are based on surface plate motions only, with no internal density heterogeneities.

an age of 100 Ma instead of 120 Ma tends to yield on the order of 10% less hot spot motion since 43 Ma [see also *Steinberger*, 2000, Figure 15; *Steinberger and O'Connell*, 2000, Figure 12]. The computed hot spot motion since 43 Ma depends slightly on assumed "age", because the tilt of a plume conduit tends to increase with time, and the buoyant rise of a tilted conduit causes hot spot motion – the more tilted, the faster – even in the absence of large-scale mantle flow. In cases 14 and 15 of Table 1, the computation yields a Hawaiian plume conduit that becomes strongly tilted and hence an unrealistically fast hot spot motion since 43 Ma is computed. In these cases, an age of 100 Ma is assumed for the Hawaiian hot spot, because this yields a somewhat smaller computed hot spot motion.

[14] Anomalous mass fluxes $B = 6.5 \times 10^3$ kg/s for Hawaii and $B = 2.0 \times 10^3$ kg/s for Louisville are assumed, based on work by *Davies* [1988], *Sleep* [1990], *Davies* [1992] and *Ribe and Christensen* [1999]. As in *Steinberger* [2000], the buoyant rising speed $u$ of the plume conduit through the

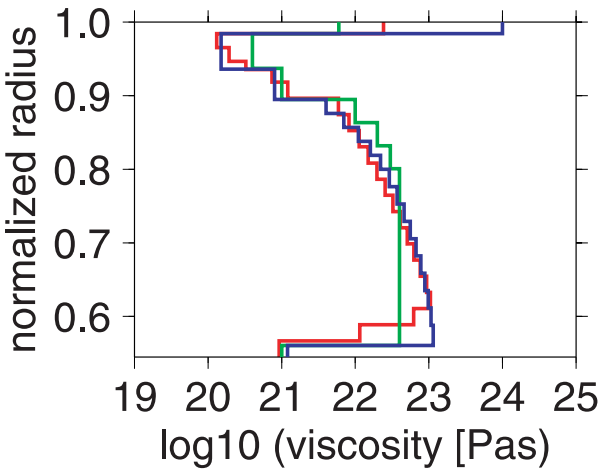


**Figure 1.** Three radial viscosity structures used in this paper. Green line used by *Steinberger* [2000] will be referred to as "Model I". Blue line is the preferred structure of *Steinberger and O'Connell* [1998] and will be referred to a "Model II". Red line is derived by *Steinberger and Calderwood* [2001] and will be referred to as "Model III".

surrounding mantle as a function of depth $z$ is then computed as

$$u(z) = u_0 \sqrt{B/B_0}\ \eta_0/\eta(z), \quad (1)$$

or

$$u(z) = u_0 \sqrt{B/B_0}\ \sqrt{\eta_0/\eta(z)}; \quad (2)$$

whereby $u_0$ is given in Table 1, $\eta(z)$ is viscosity of the ambient mantle, which is assumed to depend only on depth, $B_0$=$10^3$ kg/s and $\eta_0$=$10^{21}$ Pas. Values of $u_0$ are based on laboratory experiments [*Richards and Griffiths*, 1988] scaled to appropriate viscosities and plume diameters. The first equation corresponds to assuming a constant viscosity inside the plume, hence a constant plume radius; the second equation corresponds to viscosity inside the plume, and hence plume radius, increasing with depth, whereby the ratio of viscosity inside and outside the plume remains constant.

[15] In addition to the previous viscosity structures, we will also use a viscosity structure of *Steinberger and Calderwood* [2001], derived by optimizing the fit to geoid and heat flow constraints for mantle density and corresponding flow based on recent tomography models. It is very similar to the preferred viscosity structure of *Steinberger and O'Connell* [1998], except in the lowermost mantle. The three viscosity structures are shown in Figure 1. All of them have a rather high viscosity in the lower mantle, a feature that is required to make hot spot motion sufficiently slow, and to make computed hot spot tracks approximately match observed tracks [*Richards*, 1991; *Steinberger and O'Connell*, 1998].

[16] Figure 2 shows an example for the motion of the Hawaii and Louisville hot spots, computed as described by *Steinberger and O'Connell* [1998] with parameters as described above. It is in a direction roughly opposite to plate motion, with a magnitude on the order of 10% of plate motion. Similar results were obtained for a wide range of computations [see also *Steinberger and O'Connell*, 2000, Figure 12; *Steinberger*, 2000, Figure 15]: The computed hot spot motion tends to represent flow at mid-mantle depths [*Steinberger and O'Connell*, 2000], and tends to be in a direction opposite to plate motion. The flow field is, however, not a simple kinematic plate return flow. Kinematic flow at mid-mantle depths is strongest near the boundaries, and, especially if whole-mantle flow is assumed, rather weak beneath the interior of the Pacific plate. Computed motion of the Hawaiian hot spot is therefore largely due to an inflow to the large-scale upwelling under the south central Pacific. Hence the inferred plate motion is on the order of 10% slower than that calculated assuming fixed hot spots. These plate motions were computed with a method [*Steinberger*, 2000] that optimizes the fit to the Hawaiian and Louisville hot spot tracks and age data [*Clague and Dalrymple*, 1989; *Keller et al.*, 1995; *Watts et al.*, 1988].

[17] Table 1 shows that for a number of different assumptions the computed Pacific plate motion in a mantle reference frame is almost always slower than the motion computed assuming fixed hot spots. We have previously shown [*Steinberger and O'Connell*, 2000, Figure 8] that a motion of the Hawaiian hot spot similar to the one shown in Figure 2 is also sufficient to explain the rather small difference between the observed Hawaiian hot spot track and that predicted assuming the Hawaiian hot spot is fixed in the African hot spot reference frame, during the past 43 Ma. It is more difficult to explain the larger difference prior to 43

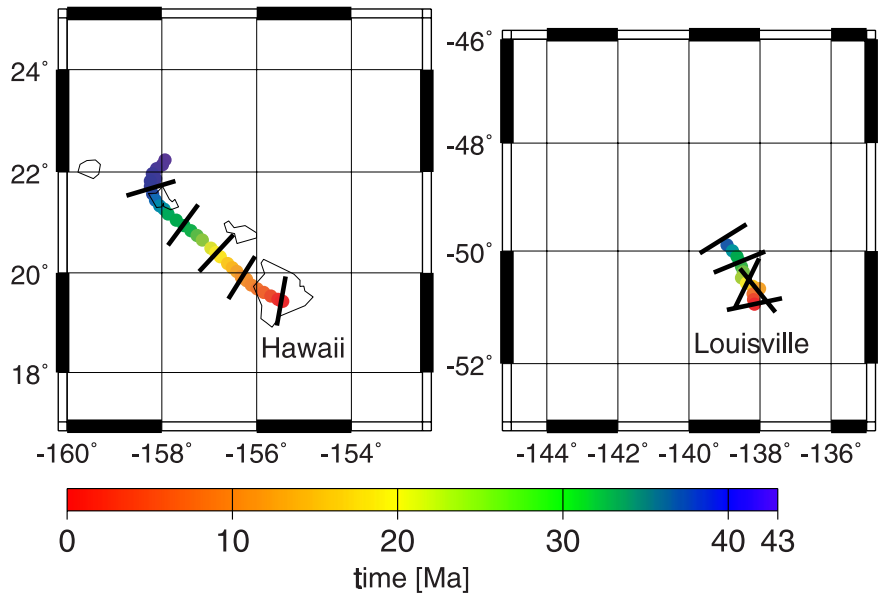


**Figure 2.** An example for the motion of Hawaii and Louisville hot spot during the past 43 Ma, computed for Case 11 of Table 1. Thick rainbow-colored lines show the computed motion of the hot spot during the past 43 Ma, which follows the line, from the purple-blue end (43 Ma ago) to the red end (present-day). The location at a given time can be inferred from the color scale, and also the tickmarks (at 10 Ma intervals).

Ma, but we restrict our attention here to the last 43 Ma, because it is unlikely that any volcanics older than that occur along the Easter hot spot track. This will be further discussed below.

[18] In most cases shown here, equation 1 is used, although the assumption on which equation 2 is based is probably more realistic: the reason for this choice is, that we previously found that both cases generally tend to give rather similar results for direction and magnitude of hot spot motion [*Steinberger*, 2000; *Steinberger and O'Connell*, 2000], but that case (1) tends to yield a somewhat more coherent motion of Hawaiian and Louisville hot spot, hence predicted tracks tend to give a better fit to the observed ones. Later on in this paper, we will show that for the more detailed modelling presented here, results for both cases remain similar. Hence it is very likely that none of the conclusions reached here would change if equation 2 was used as the standard assumption.

[19] As in the fixed hot spot case, we consider either one constant Pacific plate motion 0–43 Ma, or two constant plate motions 0–25 Ma and 25–43 Ma that give the best fit to the observed ages and shapes of the Hawaiian and Louisville hot spot tracks. In the second case, the best-fitting plate velocity 0–25 Ma tends to be about 20% faster than in the first case, both for cases with fixed and moving hot spots, similar to other results [*Raymond et al.*, 2000; *Wessel and Kroenke*, 1997]. This difference tends to be larger than differences between results for fixed and moving hot spots in the same column of Table 1.

## 3. Construction of Plate Boundary Evolution

[20] Plate motions are boundary conditions for mantle flow, hence the locations of plate boundaries influence the mantle flow field which is used to compute the motion of plumes. Furthermore, the location of plate boundaries determines on which plate(s) we expect a hot spot track. Here the digital isochrons of *Müller et al.* [1997] on the Pacific ocean floor, chrons 34 and later (available e.g. at ftp://ftp.agg.nrcan.gc.ca/products/agegrid/isochrons. dat.gz) are used to reconstruct plate boundaries in the Pacific basin during the past 84 Ma.

[21] In a first step, isochrons that are not on the Pacific plate but required to construct boundaries are rotated on to the Pacific plate, using the same

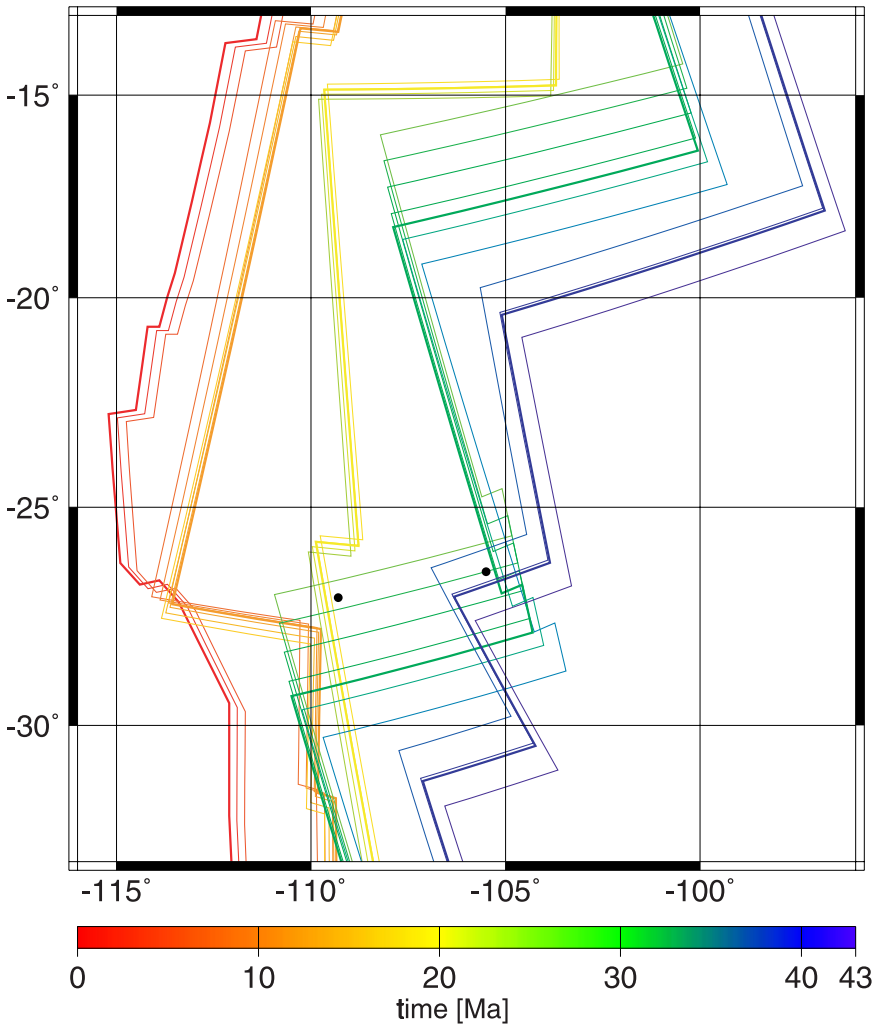


**Figure 3.** Pacific-Nazca plate boundary for the Pacific plate motion of *Duncan and Clague* [1985] for different times, represented by different colors: Thick lines correspond to the times of the isochrons used, thin lines are at 2 Ma time intervals. Black dots indicate the locations of Easter and Sala y Gomez islands.

relative plate motions that were used to construct the isochron set (*Mayes et al.* [1990], listed at http://www.es.usyd.edu.au/geology/people/staff/dietmar/Agegrid/digit_isochrons.html). In the next step, boundaries are constructed in 2 Ma intervals in the reference frame of the Pacific plate, assuming symmetric spreading. The ridge jumps introduced by this assumption are somewhat arbitrary, but in section 4.1 it will be shown that they do not affect our results in a major way, and in section 5 evidence for such ridge jumps will be discussed. After this, the computed Pacific plate motions listed in Table 1 are used to rotate the plate boundaries into the corresponding (fixed hot spot or mantle) reference frame, hence the resulting plate boundary reconstructions are different in each case. In the last step, the constructed plate boundaries in the Pacific region are connected to the plate boundaries elsewhere [*Lithgow-Bertelloni et al.*, 1993; *Gordon and Jurdy*, 1986] in order to expand the plate velocity field in spherical harmonics and compute the kinematic part of the mantle flow field.

[22] As an example, Figure 3 shows the Pacific-Nazca plate boundary computed for the Pacific plate motion of *Duncan and Clague* [1985] (Case 3 of Table 1), hence in the fixed hot spot reference frame. The boundary at different times is shown in different colors; the Nazca plate is to the right, the Pacific plate to the left of the boundary. Black

dots indicate the locations of Easter (left) and Sala y Gomez (right) Islands. Between ≈26 and 43 Ma, a hot spot location on the Pacific rather than the Nazca plate is predicted. For comparison, plate boundaries computed under consideration of hot spot motion will be shown in the next section, along with the computed motion of the Easter hot spot.

## 4. Computation of Easter Hot Spot Motion and Track

### 4.1. Hot Spot Motion

[23] The motion of the Easter hot spot is computed essentially in the same way as for Hawaii and Louisville (as described in section 2). However in most cases the plate boundary reconstructions described in the previous section are used. Also, in most cases, a regional high-resolution flow field, with the kinematic part expanded up to degree 255 and evaluated on a 0.5-degree grid is used in a region surrounding the Easter hot spot.

[24] If not mentioned otherwise, buoyant rising speed is computed using equation 1 with $B = 2.1 \times 10^3$ kg/s [*Sleep*, 1990; *Schilling*, 1991] and $u_0$ as specified in Table 1. In order to quantify the effect of rising speed, other cases are also included. An age of 100 Ma is assumed for the initiation of Easter plume activity unless stated otherwise but other cases are also included, in order to find out how hot spot motion depends on plume longevity.

[25] The figures in this section contain up to three different elements:

1. Thick rainbow-colored lines showing the computed motion of the hot spot for various cases. The computed motion of the hot spot during the past 43 Ma follows the line, from the purple-blue end (at 43 Ma) to the red end (present-day). The location at a given time can be inferred from the color scale, and also the tickmarks (at 10 Ma intervals).
2. Thinner colored lines showing the computed location of the Pacific-Nazca plate boundary for different times. The same color scale as for hot spot motion is used. In this way one can find out for any time and many of the cases shown whether the computed hot spot location is on the Nazca plate – if it is to the right of the boundary with the same color – or Pacific plate otherwise.
3. Purple arrows showing the present-day flow at mid-mantle depth. This is plotted to enable comparison of flow with hot spot motion.

All three elements are shown in the mantle reference frame introduced in the first section.

[26] Figure 4 shows some fairly typical results of our calculations. It shows the calculated hot spot motion for four different cases of buoyant plume rising speed. A hot spot motion of about 500 km during the past 43 Ma in a southwesterly direction is predicted in all cases – independent of plume rising speed. This motion is composed of a long-term motion in west-southwesterly direction and episodes of motion in east-southeasterly direction lasting a few million years. The long-term motion is caused by, and representative of, the horizontal flow component in the upper part of the lower mante, as previously explained [*Steinberger and O'Connell*, 2000]. Cases B and D have higher plume rising speeds than A and C, hence the computed hot spot motion in cases B and D tends to represent flow at greater depth than in cases A and C. Figure 4 also shows arrows representing present-day flow. The computed flow shown is dominated by a "return flow" component towards the East Pacific Rise and, under the Nazca plate, away from the subduction zone under South America, opposite to plate motion. The computed hot spot motion is actually faster than the flow field. This can be explained because the plume conduit is tilted, with the lower part of the conduit west of the surface hot spot [see, e.g., *Steinberger*, 2000, Figures 3 and 4], and located in a region of large-scale upward flow. The tilt is caused because the base of the plume moves westward with the flow in the lower part of the mantle above D" – an inward flow towards the large-scale upwelling under the presumed Pacific superswell, and faster than at mid-mantle depths, despite the higher viscosity. If such a tilted conduit is swept upwards in large-scale flow, in addition to buoyant rising, the hot spot surface motion may be faster than the flow at mid-mantle depth.

[27] The episodes of motion in east-southeasterly direction occur each time (at 25.8 and 17 Ma) that

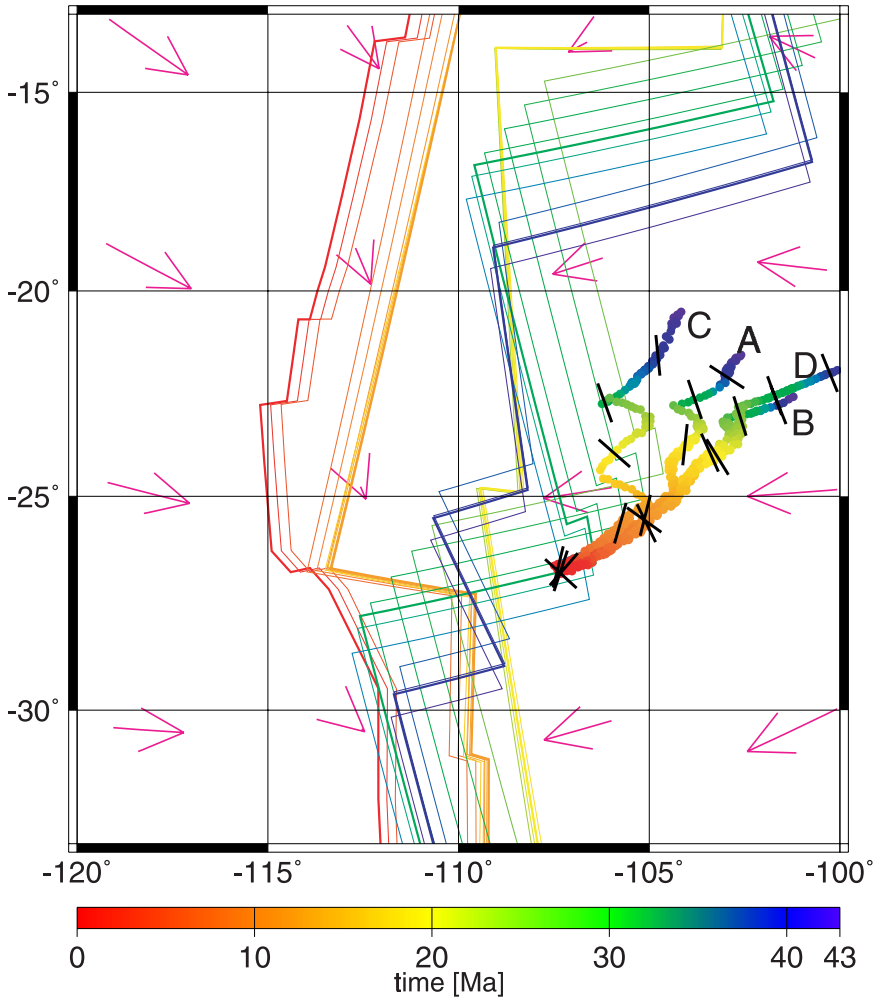


**Figure 4.** The effect of plume rising speed on the computed motion of the Easter hot spot. Calculated hot spot motion during the past 43 Ma is shown for four different cases of buoyant plume rising speed. Cases A, B and C use equation (1) with $u_0$ = 0.86 cm/yr, 1.72 cm/yr and 0.43 cm/yr respectively, whereas case D uses equation (2) and $u_0$ = 2.38 cm/yr. Other parameters are the same as in cases 13 and 22 of Table 1. A present hot spot location half-way between Sala y Gomez and Easter Island is assumed. The Pacific-Nazca plate boundary, constructed for case 13 (Table 1) with two different Pacific plate rotation rates 0–25 and 25–43 Ma, is shown with the same color scale. Thick lines correspond to the times of the isochrons used, thin lines are at 2 Ma intervals. Arrows represent the computed present-day horizontal flow field at 0.87 Earth radii (depth 828 km); 1cm/yr corresponds to an arrow length of 2 degrees of arc, i.e. the arrow length would correspond to the total motion during ≈19 Ma for constant flow.

a major ridge jump occurred. The largest changes of the flow field around the location of the plume occur at a depth of ≈250–500 km. After a few million years, which is approximately the buoyant rising time of the plume conduit through that depth interval, the plume conduit has mostly adjusted to the change in flow, and hence the episodes of motion in east-southeasterly direction last a few million years. They last longer and are more pronounced if a lower buoyant rising speed is assumed. At the location of the Easter hot spot and depths 250–500 km, the return flow gets weaker after each ridge jump, and the difference between the flow fields before and after the ridge jump is in an east-southeasterly direction, which is the hot spot motion after the ridge jump. After these episodes, the hot spot motion again represents flow in the upper part of the lower mantle (as the buoyant rising speed of the plume conduit through that region of higher viscosity is much longer, of the order of the plume age, ≈100 Ma), plus the rising of a tilted conduit supported by

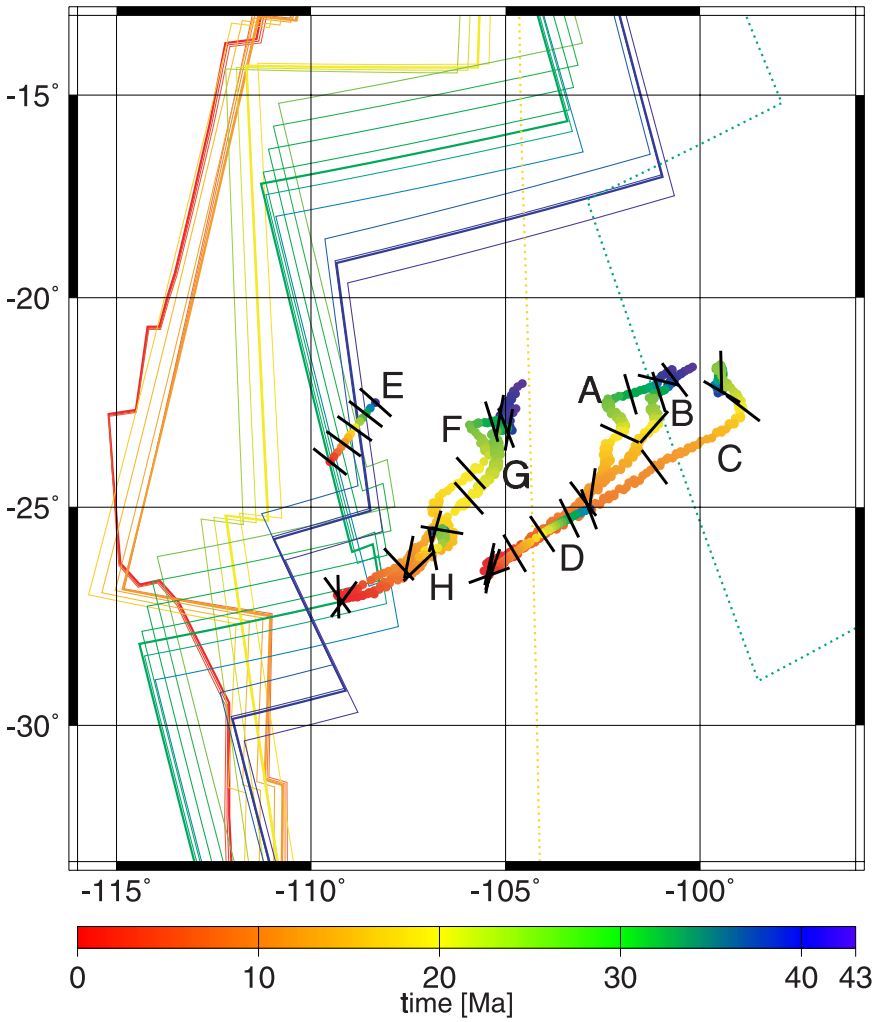


**Figure 5.** Effect of the Pacific-Nazca plate boundary location and "sharpness" on the computed motion of the Easter hot spot. Hotspot motion during the past 43 Ma is shown, computed for case 13 of Table 1 and different plate boundary locations and flow fields. (A) and (F): Plate boundary was computed for constant Pacific plate motion 0–43 Ma. This plate boundary reconstruction is shown as continuous lines with the same color scale; thick lines correspond to the times of the isochrons used; thin lines are at 2 Ma time intervals. (B): Plate boundary was computed for two different Pacific plate stage poles, 0–25 and 25–43 Ma (shown in Figure 4). (C): previous plate boundary [*Lithgow-Bertelloni et al.*, 1993; *Gordon and Jurdy*, 1986]. This reconstruction has constant boundaries 0–10 Ma (as present-day, red line), 10–25 Ma (yellowish dotted line), and 25–43 Ma (greenish dotted line). (D) and (E): constant plate boundary (40 Ma, blue line). (G) and (H): as F, but flow field is expanded only up to degree 31 for (G) and degree 15 for (H). Present hot spot location is assumed at Sala y Gomez Island in cases A, B, C and D, at Easter Island in cases F, G and H. The location for case E is chosen such that the hot spot crosses beneath the plate boundary.

large-scale flow. If in reality there has been asymmetric spreading instead of ridge jumps, the corresponding component of hot spot motion would also be more "smeared out" over time.

[28] At least for the viscosity structures used here, which all have a low viscosity channel beneath the lithosphere, and viscosity below increasing with depth, the plume tilt due to shear flow in the direction of plate motion immediately beneath the lithospheric plates, [*Richards and Griffiths*, 1988], is rather small: Flow in the direction of plate motion is restricted to a rather narrow depth interval with low viscosities, and the buoyant rise time of the plume through that low-viscosity depth interval is only of the order of 1 Ma, hence the plume is not much tilted in this low-viscosity channel. This is illustrated by case E in Figure 5,

where for simplicity a constant ridge location (40 Ma, i.e. the thick blue line) and flow field is assumed, and a plume location such that the ridge crosses the plume. If the plume was tilted over in the direction of the plate motion by several 100 km, there would be a visible effect as the plume crossed beneath the plate boundary, because the kinematic flow field is expanded up to degree 255, such that the imposed surface velocity changes by about 20 cm/yr over <100 km across the boundary. However there is no such effect visible.

[29] Other results included in Figure 5 show the effect of which plate boundary location is used to compute the flow field and to what degree the flow field is expanded. The inferred past boundary between Pacific and Nazca plate depends on Pacific plate motion, with slower motion corresponding to a boundary farther west in the past. This can be seen by comparison of Figures 3 and 5. The magnitude of the ridge jumps is obviously the same in both cases. Comparison of cases A and B shows that the uncertainties of the plate boundary location arising from uncertainties in Pacific plate motion lead to rather small differences in the computed hot spot motion. Differences between plate boundary locations in Figures 4 and 5 for the same times are similar in magnitude to ridge jumps required in the case of symmetric spreading. Hence the overall differences between hot spot motion displayed here and corresponding computations with gradual ridge migration would be similar in magnitude to the difference between cases A and B in Figure 5. However without ridge jumps the curves of computed hot spot motion would presumably have no sharp kinks. Comparison with case C, which uses the plate boundary adopted in our previous computations [e.g., *Steinberger*, 2000] and also shown in Figure 5, shows that even though that plate boundary is rather different, the overall predicted hot spot motion during the past 43 Ma is still rather similar.

[30] Thus, previously computed results of Easter hot spot motion are qualitatively still valid despite the use of an inaccurate plate boundary reconstruction. Case D is like case E computed for a constant ridge location (40 Ma, thick blue line). The predicted direction of hot spot motion is still the same as for cases A, B and C, but the magnitude is somewhat smaller. This can be explained because most of the time hot spot motion represents flow in the upper part of the lower mantle, and at that depth the horizontal flow component within a few 100 km of the ridge tends to be weaker than farther away (see, e.g., Figure 4), as the flow field becomes increasingly vertical. For case D, the hot spot is always within ~500 km of the ridge, whereas for the other cases it tends to be farther away, therefore the predicted hot spot motion is smaller for case D than for A, B and C. The same effect (that a hot spot location close to the ridge corresponds to slow hot spot motion) can also be seen in cases E and C: In case C, the hot spot is initially very close to the ridge and moves very little, and later, especially during the past 10 Ma, is rather far from the ridge, and moves rather fast.

[31] Cases F, G and H show the effect of spherical harmonic expansion of the flow field: For case F, like most other cases, the kinematic part of the flow field is expanded up to degree 255 and evaluated on a 0.5 degree grid above a depth of 637 km, whereas in case G the flow field is expanded to degree 31. The two cases show very little difference, because shear flow in the direction of plate motions in the uppermost mantle has very little influence on hot spot motion, and at depths where the flow field has a larger effect on hot spot motion, expansion of the flow field up to degree 31 (≈1200 km wavelength) is already quite accurate. However, if the flow field is expanded only up to degree 15 (≈2500 km wavelength), computed hot spot motion is considerably less, because the gradient of the flow close to the East Pacific rise in the upper part of the lower mantle is not appropriately modeled. In contrast, it was found that for most other hot spots – which are not close to a fast spreading ridge – the computed motion for expansion to degree 15 is rather similar to that for degree 31. For that reason, flow fields were expanded only up to degree 15 for the computation of Hawaiian and Louisville hot spot motion in section 2.

[32] Figure 6 shows, based on a different tomography model, how computed hot spot motion gets stronger for older initiation of hot spot activity. This occurs because hot spot motion tends to

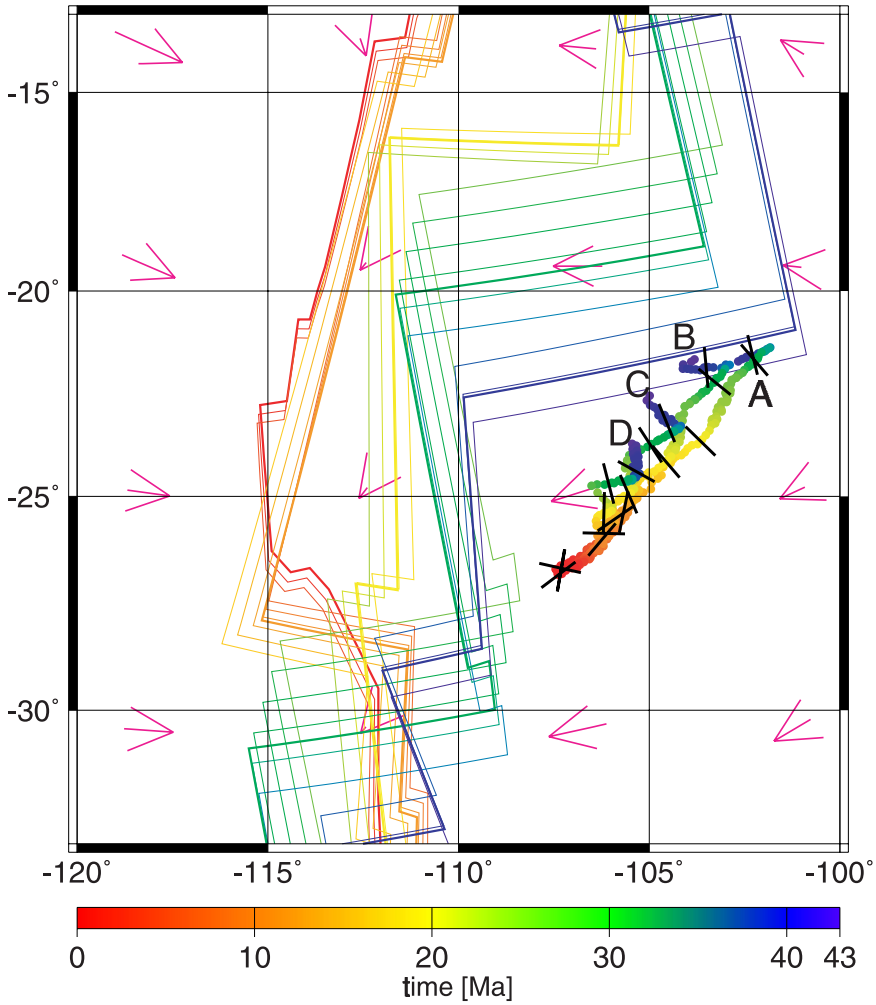


**Figure 6.** The effect of assumed hot spot age on the computed motion of the Easter hot spot. Hot spot motion during the past 43 Ma is shown, computed for Case 10 of Table 1, with plate boundaries for constant Pacific plate rotation rate 0–43 Ma. The Pacific-Nazca plate boundary used is shown with the same color scale. Thick lines correspond to the times of the isochrons used, thin lines are at 2 Ma time intervals. Assumed ages are (A) 120 Ma, (B) 100 Ma, (C) 80 Ma, and (D) 60 Ma. Arrows represent the horizontal flow field at depth 800 km, with a length scale as in Figure 4.

reflect flow at greater depth with increasing age since initiation, and the flow beneath the Easter Island region gets stronger with depth, in the lower mantle. In addition, an initially vertical plume conduit becomes more tilted with age, hence the effect of a tilted plume conduit rising to the surface also gets stronger.

[33] Figure 7 shows, based on yet another tomography model, the effect of plume location. The computed overall hot spot motion is similar for all three cases, but it is somewhat faster for an assumed hot spot location farther away from the ridge, as at this location the return flow towards the ridge in the upper part of the lower mantle tends to be stronger. Also the "kinks" in the predicted motion, which are caused by changes of flow in the lower part of the upper mantle due to ridge jumps, get less pronounced if the plume is farther away from the ridge. Figure 8 shows for two different tomography models, that the results do not depend much on which of the three viscosity structures is used.

[34] We showed results for some different density models in the previous figures. Figure 9 focuses on this comparison, with results based on 5 different tomography models: four recent models plus the model by *Su et al.* [1994], which we had frequently used in our previous papers, and one case not based

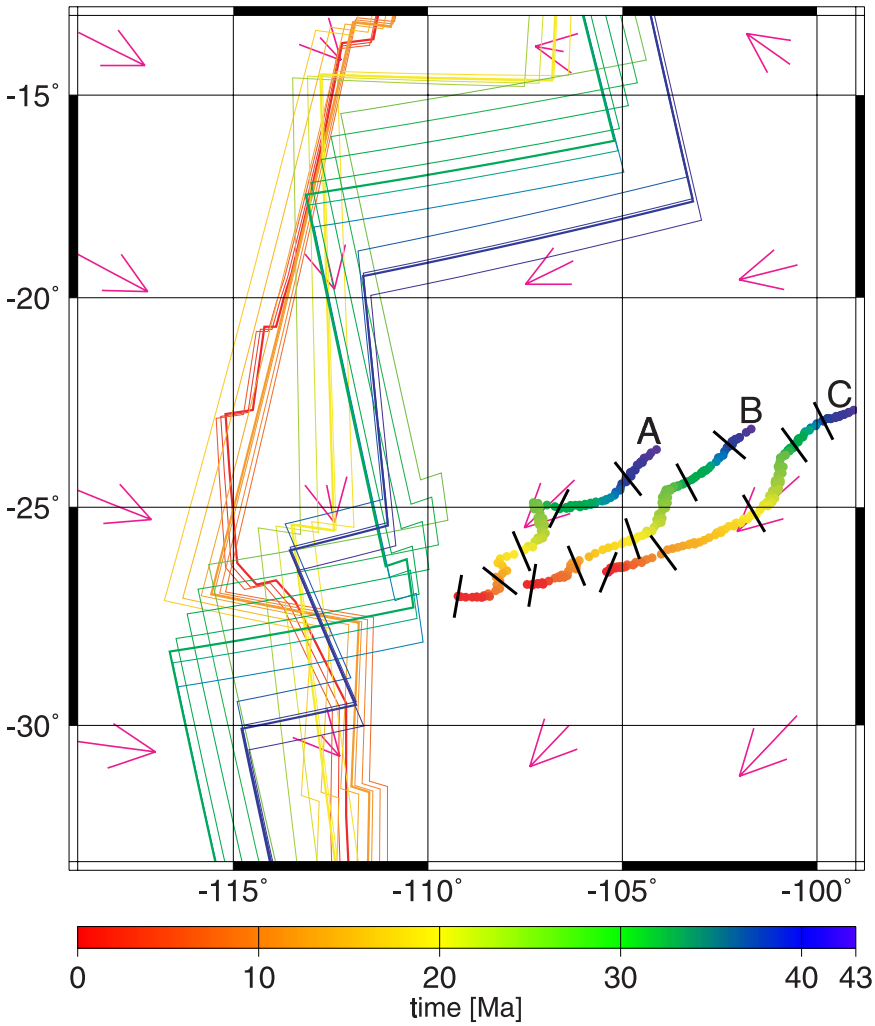


**Figure 7.** The effect of assumed present-day hot spot location on the computed motion of the Easter hot spot. Hot spot motion during the past 43 Ma is shown, computed for Case 6 of Table 1, with plate boundaries for constant Pacific plate rotation rate 0–43 Ma. The Pacific-Nazca plate boundary used is shown with the same color scale. Thick lines correspond to the times of the isochrons used, thin lines are at 2 Ma time intervals. Assumed present-day hot spot locations are (A) at Easter Island (B) half-way between Easter and Sala y Gomez Island (C) At Sala y Gomez Island. Assumed hot spot age is 120 Ma. Arrows represent the horizontal flow field at 0.87 Earth radii (depth 828 km), with a length scale as in Figure 4.

on tomography. Four out of the five tomography models, including the one by *Su et al.* [1994], yield rather similar results, and the fifth model still yields a similar direction of hot spot motion, but at a considerably slower velocity. Resolution of tomographic models is limited by ray coverage, and the Pacific is rather poorly covered in body-wave models, hence resolution is low [e.g., *Bijwaard et al.*, 1998]. For that reason, we also include one case not based on tomography. In contrast to the other cases, the flow field in case 21 is based on surface plate motions only, with no internal density heterogeneities. Also, layered convection is assumed; i.e., all the kinematic return flow is restricted to the upper mantle, and consequently the plume is assumed to originate at the 670 km discontinuity. Hence computed hot spot motion mostly represents flow at that depth. It can be seen that even for this rather different case, the predicted direction of hot spot motion is still rather similar, but its magnitude is smaller than for most flow fields based on mantle density models. Qualitatively the smaller magni-

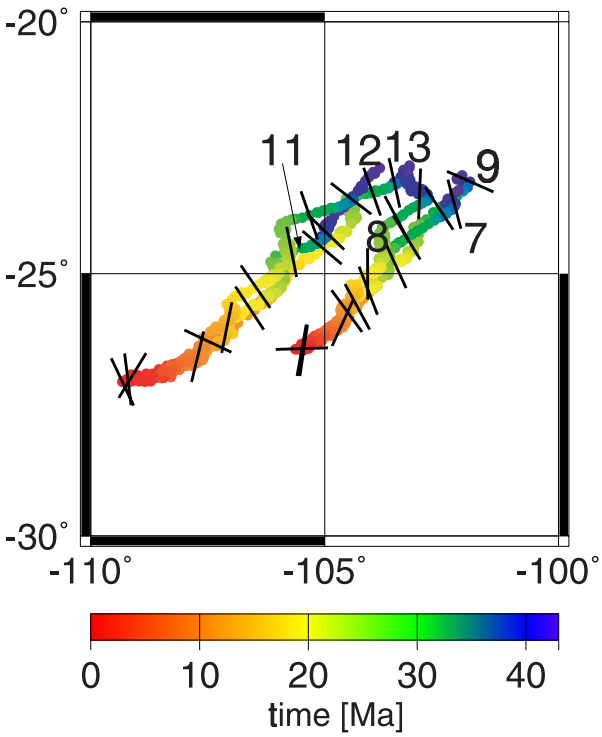


**Figure 8.** Computed motion of the Easter hot spot for different mantle viscosity structures. Hot spot motion during the past 43 Ma is shown, computed for cases similar to 11–13 and 7–9 (as indicated) of Table 1, with the only difference that $u_0$ is twice as large for the Easter plume. Corresponding plate boundaries for constant Pacific plate rotation rate 0–43 Ma are used. Assumed present-day hot spot locations are at Easter Island for cases 11–13 and at Sala y Gomez Island for cases 7–9. Assumed hot spot age is 100 Ma.

tude can be explained because in this case computed hot spot motion does not contain a contribution from a rising, tilted conduit.

[35] Finally, Figure 10 shows that phase boundaries, compressibility and advection of mantle density anomalies have rather small effects on the computed hot spot motion.

## 4.2. The Easter Hot Spot Track on Nazca Plate

[36] In order to allow a direct comparison with data, the tracks on the Nazca plate corresponding to the calculated Easter hot spot motion described in the previous section, or alternatively assuming a fixed Easter hot spot, are computed. The re-computed Pacific plate motion described in section 2, and the relative motion of Pacific versus Nazca plate from *Tebbens and Cande* [1997], which are partly based on *Cande et al.* [1995] and *Pardo-Casas and Molnar* [1987] are used, in combination with the timescale of *Berggren et al.* [1995]. Since the reconstructions of *Tebbens and Cande* [1997] go back only to anomaly 13, tracks are plotted only to 33 Ma, but this is sufficient for the purpose of this paper.

[37] A hot spot track can be created on the Nazca plate over a given period only if the plume was beneath the plate at that time. The tracks shown in this section are computed under this assumption. The figures in the previous section show that this is almost always the case for the computed hot spot motions. In contrast, the Pacific-Nazca boundary given by *Lithgow-Bertelloni et al.* [1993], which we used in our previous work, is much farther east

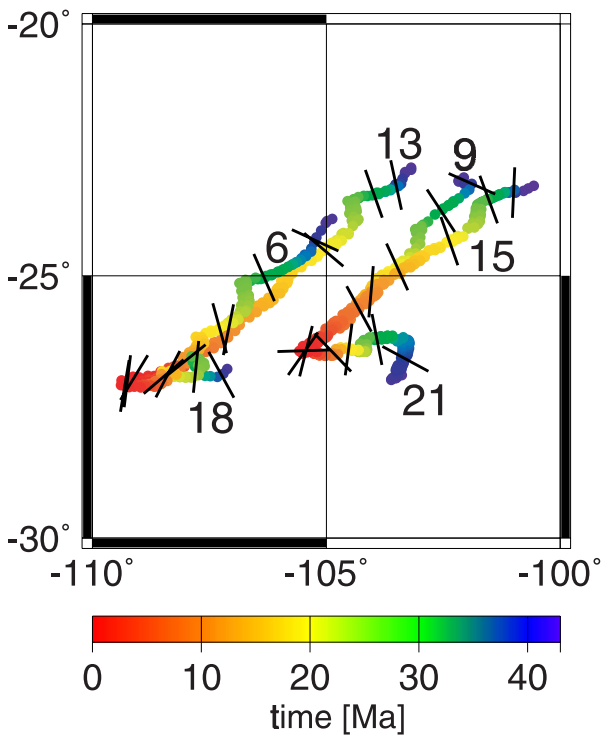


**Figure 9.** Computed motion of the Easter hot spot for different density models and flow fields. Hot spot motion during the past 43 Ma is shown, computed for cases similar to 6, 9, 13, 15, 18 and 21 of Table 1, with the only difference that $u_0$ is assumed twice as large for the Easter plume. Plate boundaries for constant Pacific plate rotation rate 0–43 Ma are used. Case numbers are indicated. For better visibility, a present-day hot spot location at Easter Island is assumed for cases 6, 13 and 18, whereas a location at Sala y Gomez Island is assumed for cases 9, 15 and 21.

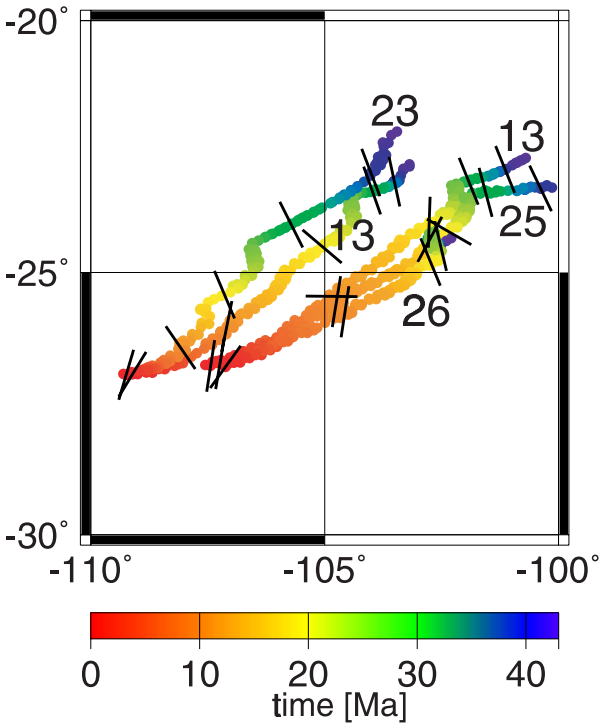


**Figure 10.** Effects of other assumptions on the computed motion of the Easter hot spot. Hot spot motion during the past 43 Ma are shown, computed for cases similar to 13, 23, 25 and 26 of Table 1, with the only difference that $u_0$ twice as large is assumed for the Easter plume. Plate boundaries for constant Pacific plate rotation rate 0–43 Ma are used. Case numbers are indicated. Two different present-day hot spot locations at Easter Island and half-way in between Easter and Sala y Gomez Island are used for better visibility.

between 10 and 43 Ma (Figure 5), therefore in combination with that boundary, prior to 10 Ma a plume location beneath the Nazca plate is predicted only in some cases [see, e.g., *Steinberger and O'Connell*, 2000, Figure 13]. Using that plate boundary, we concluded that some of the complications in the hot spot track might by due to ridge jumps, with parts of the hot spot track being transferred from the Pacific to the Nazca plate. With the plate boundaries used here, it becomes clear that such an interpretation is not viable, since the Easter hot spot was always beneath the Nazca plate during the past 43 Ma.

[38] However, even if hot spot motion is not considered, different tracks may be computed: Figure 11 shows various tracks computed for assuming fixed hot spots. The differences result from uncertainties in the age progression and shape of the Hawaii and Louisville hot spot tracks. In all cases, ages significantly older than the radiometric age dates are computed. However, computed ages roughly match the isochron ages along the Nazca ridge, i.e. a plume location roughly beneath the ridge at the time of formation of the Nazca ridge is computed. There is considerable spread among the computations, and the slower the Pacific plate motion 0–25 Ma is assumed, the better is the agreement with age data. In this figure, a hot spot location half-way between Easter Island and Sala y Gomez Island was assumed. Obviously the difference between predicted and measured ages can be further reduced if a hot spot location around Sala y Gomez Island is assumed. For the younger part, in most cases a track south of the Sala y Gomez ridge main trend (shown schematically in Figure 12) is predicted. Only for the Pacific plate motion of *Wessel and Kroenke* [1997], which changes 3 Ma ago, based on the direction of the Hawaiian Island chain, a track further north is predicted. It is therefore obvious that a rather good fit of this part of the track can be obtained by choosing an intermediate Pacific plate motion, which changes 3–5 Ma ago, but not quite as dramatically as proposed by *Wessel and Kroenke* [1997]. For the older part, in all cases the change from a NW-SE Nazca ridge to an E-W Sala y Gomez ridge is predicted. However, in none of the cases is a kink in the hot spot track predicted. The predicted trends pass well to the north of the kink in the Sala y Gomez ridge main trend shown schematically in Figure 12. This will be discussed further in the next section.

[39] Figure 12 shows computed tracks that include the effect of hot spot motion based on various computations of mantle flow. Again, a hot spot location half-way between Easter and Sala y Gomez Islands is assumed. The variation among results is rather large, as both Pacific plate motion and Easter hot spot motion vary among computations. Results tend to fit the available age data better than for fixed hot spots. The average age progression shown in Figure 12 is about 2–3 cm/yr faster than in Figure 11, because this is the relative motion of the Easter hot spot towards Hawaii and Louisville hot spots that typically results in our computations.

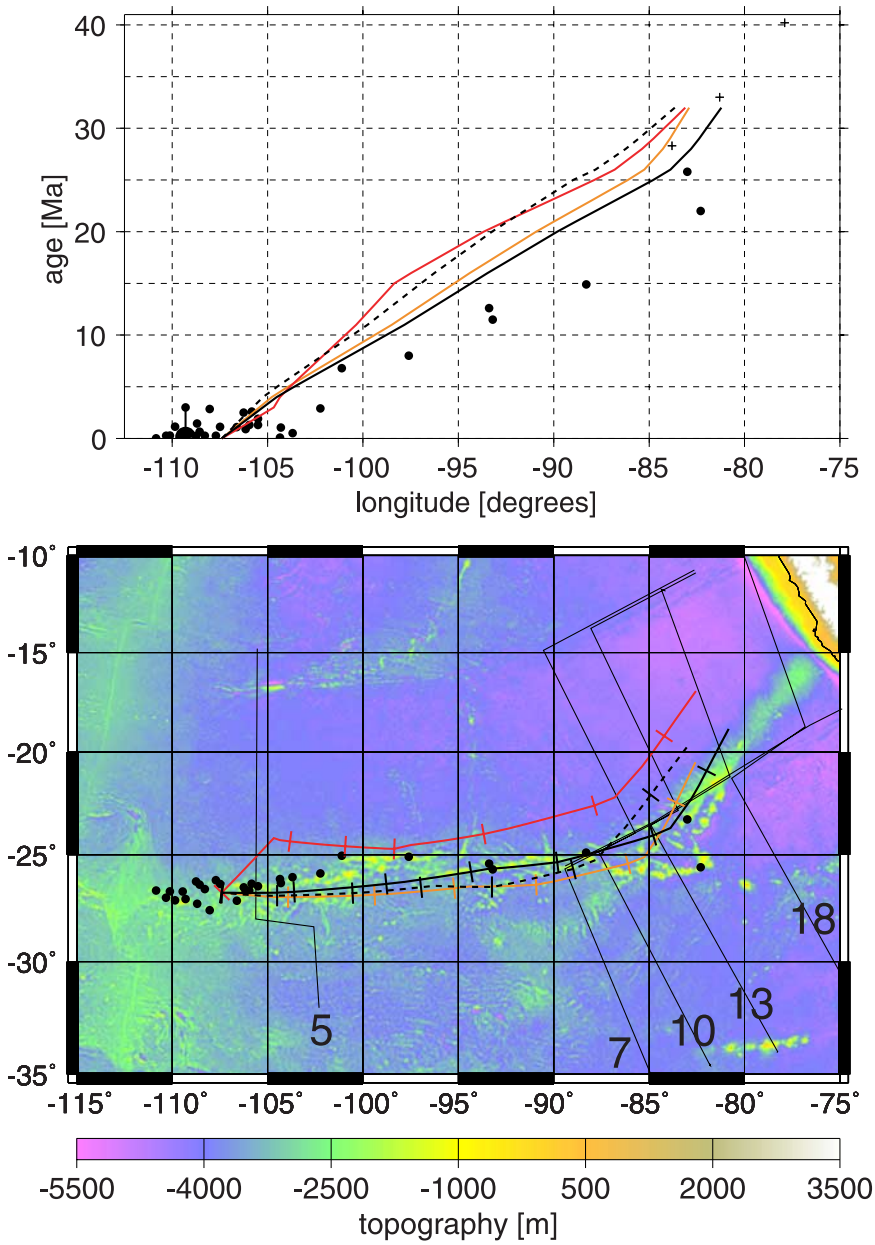


**Figure 11.** Computed Easter hot spot track and age progression (time versus longitude) on the Nazca plate for various cases of Pacific plate motion computed assuming fixed hot spots. Relative motion of Pacific versus Nazca plate is from *Tebbens and Cande* [1997] in all cases. Pacific plate motion from *Duncan and Clague* [1985] (orange line). Pacific plate motion from *Wessel and Kroenke* [1997] (red line). Best fitting Pacific plate motion – this work, case 1 of Table 1, fit is optimized for two different rotation rates 0–25 and 25–43 Ma (black dashed curve). Best fitting Pacific plate motion – this work, case 1 of Table 1, fit is optimized for constant rotation rate 0–43 Ma (black continuous curve). Tickmark interval is 5 Ma. Black dots indicate locations of dated samples and age data from *O'Connor et al.* [1995], Figure 1 (including earlier data – see there for original references) and David Naar (unpublished data). Black crosses indicate isochron ages along the Nazca ridge. Also shown are topography from the GTOPO30 data set [*Smith and Sandwell*, 1997] and magnetic anomalies from *Mayes et al.* [1990].

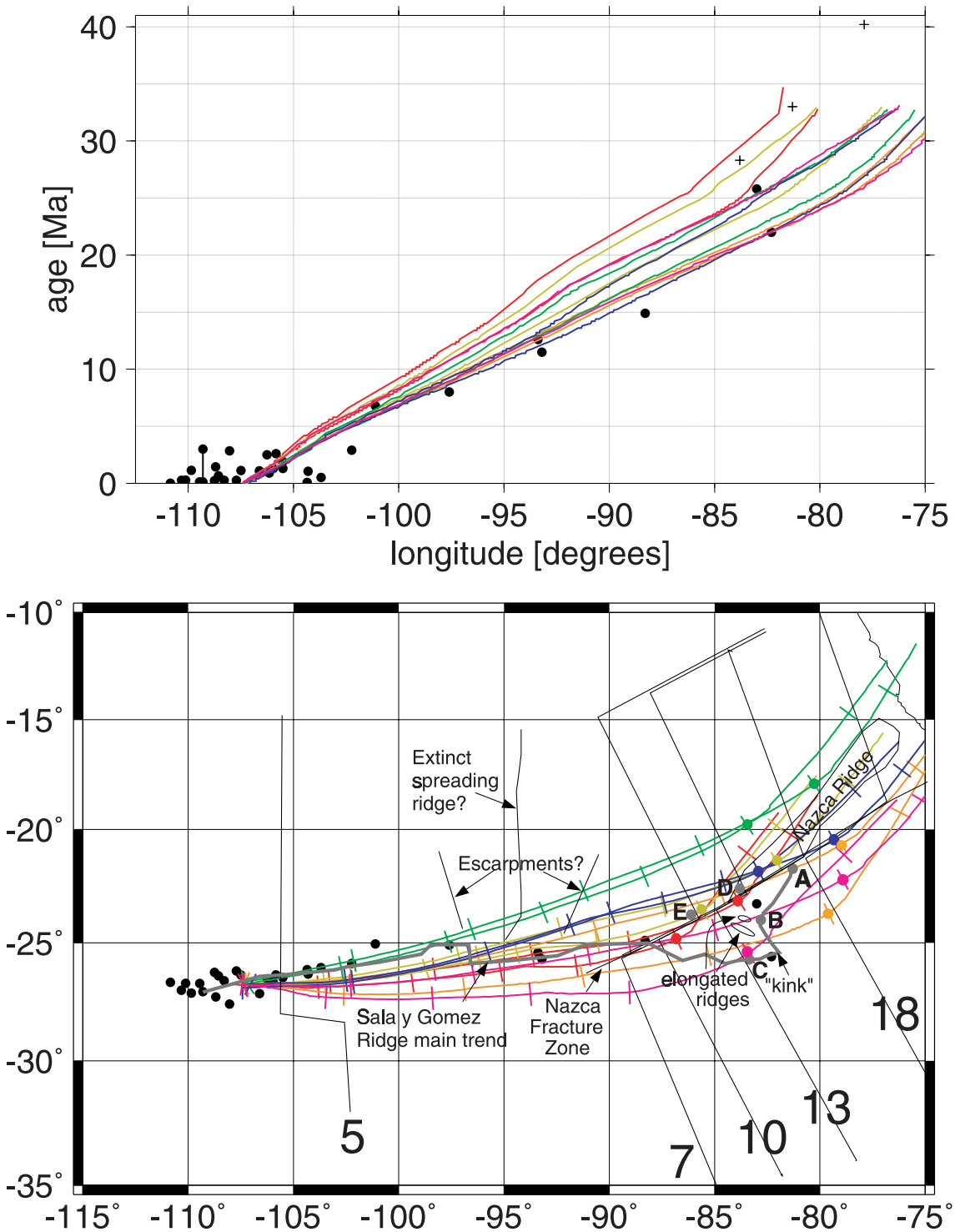


**Figure 12.** Easter hot spot track and age progression on the Nazca plate for various cases of Pacific plate motion (from Table 1) and corresponding Easter hot spot motion. Case 18 (red); Case 15 (orange); Case 21 (beige); Case 10 (green); Case 13 (blue); Case 6 (magneta). Assumed age of Easter hot spot 120 Ma. For each case, there are two lines in each panel, one for constant Pacific plate motion 0–43 Ma (leading to a faster predicted age progression on the Nazca plate between 0 and 25 Ma), and one for two different Pacific plate stage poles, 0–25 and 25–43 Ma (with slower age progression). Tickmark interval is 5 Ma, the 25 Ma point for each case is highlighted by a dot of the same color. Black dots and crosses are explained in Figure 11. Also shown is a schematic illustration of topographic features and locations mentioned in text, and magnetic anomalies from *Mayes et al.* [1990].

[40] Except for the "kink", the observed track lies within the spread of the computed tracks plotted: As an example, results for 25 Ma are plotted as colored dots. Point B on the track, which is expected to correspond to about 25 Ma according to radiometric age and the scenario proposed in the discussion section, lies within an elliptical region where the colored dots cluster. As mentioned above, these tracks are computed assuming the hot spot is always beneath the Nazca plate. This is indeed very nearly always the case, as points on the tracks for a given time are almost always to the east of the isochrons for the same time. For example, all the colored dots for age 25 Ma are to the east of chron 7 (≈25.8 Ma).

[41] Figure 13 shows some of the best fits achieved. A number of different combinations of assumptions can lead to similar fits. Therefore it is not possible to decide on one specific "preferred model". Within the models tested, it is not possible to obtain a significantly better fit. Compared to the observed track, the best fitting computed tracks tend to be too far south for the younger part of the track, and too far north around the bend between Sala y Gomez and Nazca ridge. As already explained for Figure 11, the misfit for the younger part can be reduced by a slight modification in Pacific plate motion, which will additionally improve the fit to the youngest part of the Hawaiian hot spot track. To reduce the misfit around the bend is not possible by such simple means.

### 4.3. Easter Hot Spot Track on Pacific Plate?

[42] Whereas an Easter hot spot location beneath the Pacific plate between ≈26 and 43 Ma is predicted if fixed hot spots are assumed (Figure 3), the hot spot is always, or at least most of the time, located beneath the Nazca plate during the past 43 Ma, if likely hot spot motion is considered, in combination with the respective plate boundaries (Figures 4–7). As will be discussed in the next chapter, this may well also have been the case prior to ≈43 Ma. Therefore, there may not be any actual Easter hot spot track on the Pacific plate except for features caused by interaction of plume and ridge, such as the eastern part of the Tuamotu Island platform (circled in Figure 14). Other islands and seamounts on the Pacific plate farther to the east, such as Gambier Islands and the seamounts between them and the East Pacific Rise may be unrelated to the Easter hot spot. Previously, features on the Pacific plate, especially Tuamotu and Line Islands, have been attributed to the Easter hot spot [*Morgan*, 1972]. However, obtaining a geometric fit required assuming that the Easter hot spot is presently located west of Easter Island, beneath or close to the East Pacific Rise. As is evident from the discussion of the last section, such an assumed location would worsen the misfit of the age progression on the Nazca plate, and is also unsupported by geochemical data. Furthermore, age data from Line Islands as compiled by *Duncan and Clague* [1985] do not follow a simple age progression, and they are younger than ages computed for a fixed hot spot beneath Easter Island. This misfit gets worse if hot spot motion is considered, because the Easter hot spot moves westward relative to Hawaii and Louisville according to the computations. Therefore, we conclude that the Easter hot spot did not leave a track on the Pacific plate except features caused by interaction of plume and ridge. These issues will be discussed further in the following chapter.

## 5. Discussion

[43] In this paper, a more detailed and extensive numerical modeling of hot spot motion due to mantle flow is conducted, with particular emphasis on the Easter hot spot. This hot spot was chosen because our previous model results indicated that it should move at a rate of several cm/year relative to hot spots on the Pacific plate. This predicted motion is fast enough that, based on age data along the hot spot track, it should be possible to confirm or reject the prediction. The small set of age data available so far can in fact be better explained by a hot spot moving westward relative to Hawaii and Louisville hot spots at a rate of several cm/year than by a fixed hot spot. E.g., in the top panel of Figure 11, at age 20 Ma, the best fitting line through the age data points is offset by more than 5 degrees (500 km) from all the fixed hot spot model predictions. A particular motivation for this

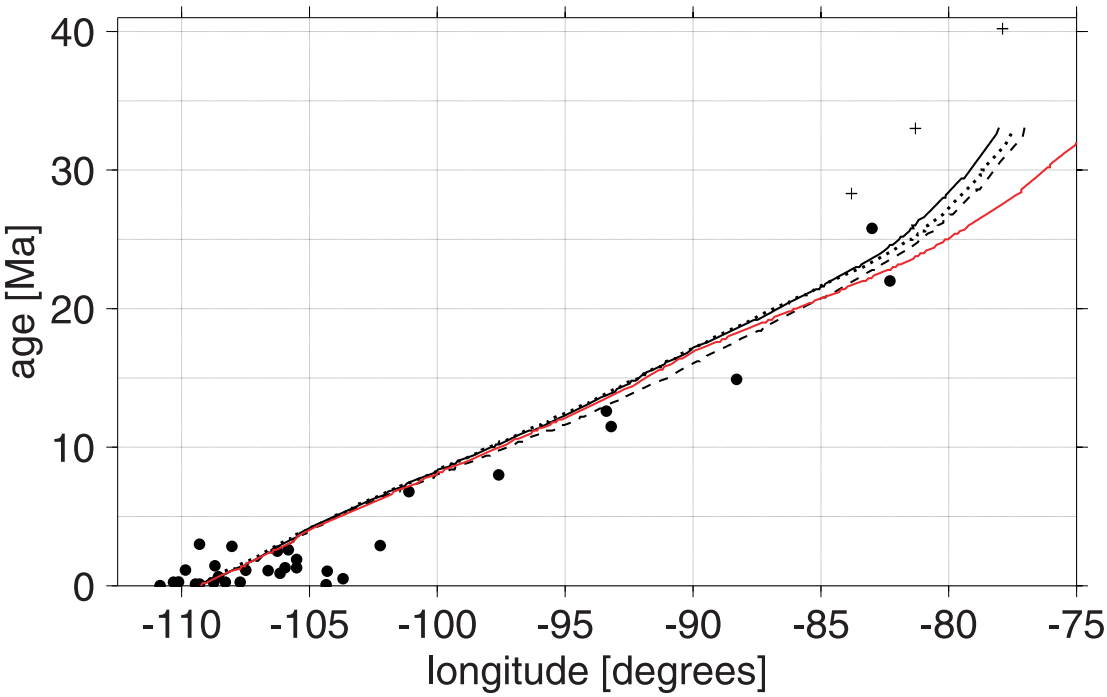
40
30
20
10
0
age [Ma]
-110
-105
-100
-95
-90
-85
-80
-75
longitude [degrees]

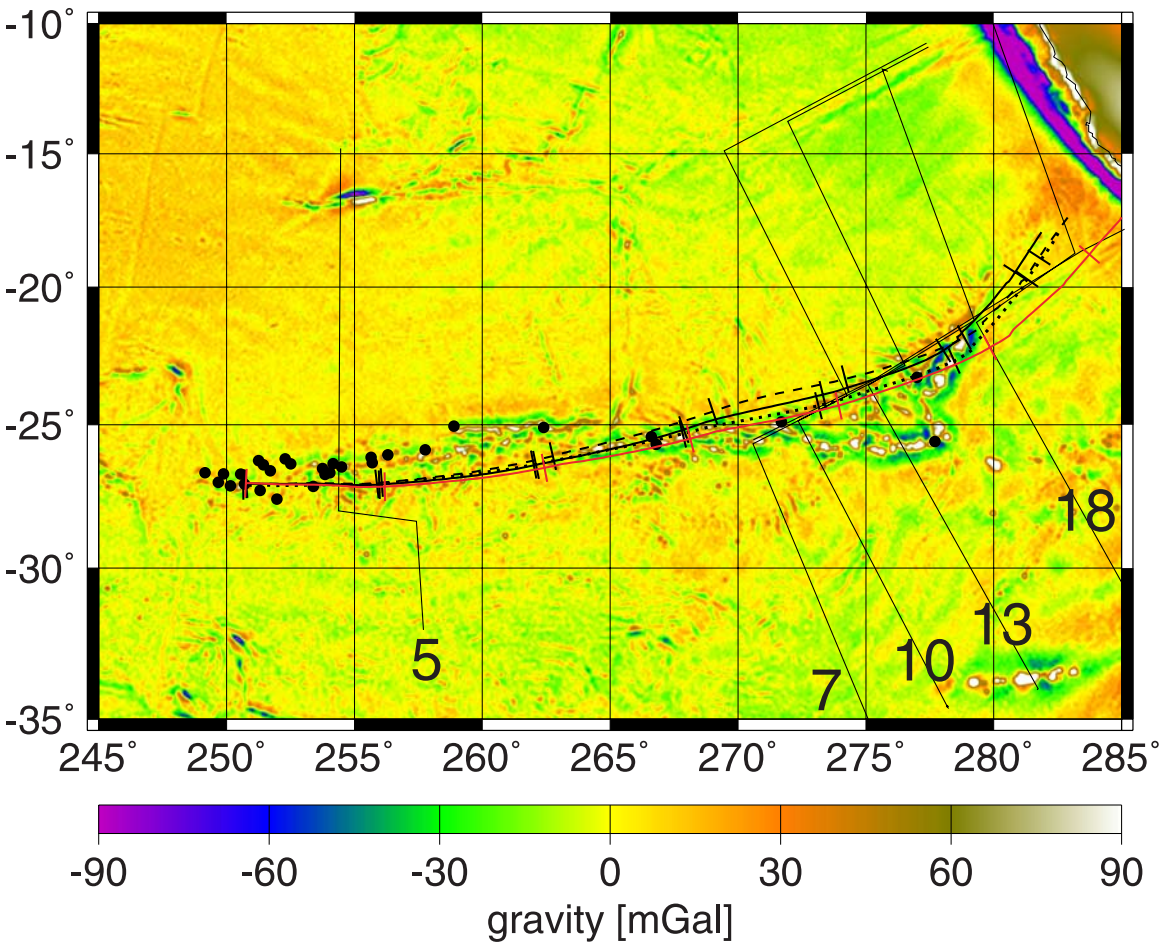
-10°
-15°
-20°
-25°
-30°
-35°
245°
250°
255°
260°
265°
270°
275°
280°
285°
5
7
10
13
18
-90
-60
-30
0
30
60
90
gravity [mGal]

work was provided by the Drift Expedition Leg 6 of the R/V Roger Revelle (Nov/Dec 2001) which dredged datable rocks from the Easter hot spot chain on the Nazca plate. A larger number of age determinations from this volcanic lineament will be available soon (David Naar et al., unpublished web manuscript at http://imina.soest.hawaii.edu/wessel/drft06rr/).

[44] Compared to our previous work, the present work represents an advance in both the modeling technique, as we have included a more accurate reconstruction of the evolution of the East Pacific Rise, and the realism of the model, as the dependence of the results on various assumptions has been tested. The results of this paper essentially confirm the previous results, in that, based on comparing the upper panels of Figures 11–13, our "best guess" of Easter hot spot motion relative to Hawaii and Louisville is about 2–3 cm/yr towards the west, which is the principal conclusion of this paper. This is composed of about 1 cm/yr east-to southeastward motion of the Hawaii and Louisville hot spots (Figure 2, Table 1) and about 1–2 cm/yr west-to southwestward motion of the Easter hot spot (Figures 4–10), in a mantle reference frame.

[45] The computed relative motion gets larger, if a greater rising speed is assumed (Figure 4), if an earlier initiation age of the Easter hot spot is assumed (Figure 6), or if a location farther away from the ridge, i.e. closer to Sala y Gomez than Easter Island (Figure 7) is assumed. Uncertainties in the assumptions lead to considerable differences among various computations of hot spot motion. When converting the computed hot spot motion to a predicted hot spot track, the uncertainties of the Pacific plate motion relative to Hawaii and Louisville, and the differences among various computations of the motion of these hot spots also become important. Hence there is a large spread among the predicted tracks and age progressions (Figures 12 and 13), and comparison with observations may actually help to constrain some of the assumptions made. For example, if greater buoyant rising speed is assumed (meaning the hot spot motion tends to represent flow at greater depth) a more southerly hot spot track that fits the observed track better, and thus may be more realistic, is usually computed (Figure 13). As another example, using the *Wessel and Kroenke* [1997] Pacific plate motion (such as in Figure 11) makes it very difficult to get a track that follows the observed trend, regardless of hot spot motion. However, Figure 11 also indicates that a Pacific plate motion that is intermediate between *Wessel and Kroenke* [1997] and other fits can give a better fit for the younger part of the Easter track. Also Figure 12 shows that, if Pacific plate motion were more or less constant during the past 43 Ma, a better fit to the available age data on the Nazca plate can be obtained than for two-stage Pacific plate motion. The available age data can be easier fit if the current plume location is not directly beneath Easter Island but somewhat farther east, as predicted previously from geochemical observations. It needs to be reiterated, though, that there are tradeoffs, with almost equally good fits for various combinations of assumptions. Therefore, any constraints on assumptions necessarily remain somewhat vague, and should be combined with other evidence. Furthermore, interpretation of radiometric ages is not really straightforward either: They may be either older or younger than ages of material erupted directly above the plume for several reasons. Volcanism can stay active for some time after the plate has moved over the plume ("postshield"), and the rocks most likely dredged from the ocean floor will be the ones erupted last at a given location. On the other hand, volcanism in the Easter chain may occur at a location before it has actually passed over the hot spot due to channeling of plume material to the spreading ridge.

**Figure 13.** (opposite) Easter hot spot track and age progression on the Nazca plate for cases 26 (black lines) and 22 (red line) of Pacific plate motion (from Table 1) and three cases of corresponding Easter hot spot motion. Assumed age of Easter hot spot 100 Ma, normal buoyant plume rising speed as specified in the text and Table 1 (continuous lines). Assumed age of Easter hot spot 120 Ma, normal buoyant plume rising speed (sashed black line). Assumed age of Easter hot spot 100 Ma, buoyant plume rising speed twice as fast (dotted black line). Tickmark interval is 5 Ma. In all cases a constant Pacific plate motion 0–43 Ma is assumed. Black dots and crosses are explained in Figure 11. Also shown are gravity from *Sandwell and Smith* [1997] and magnetic anomalies from *Mayes et al.* [1990].

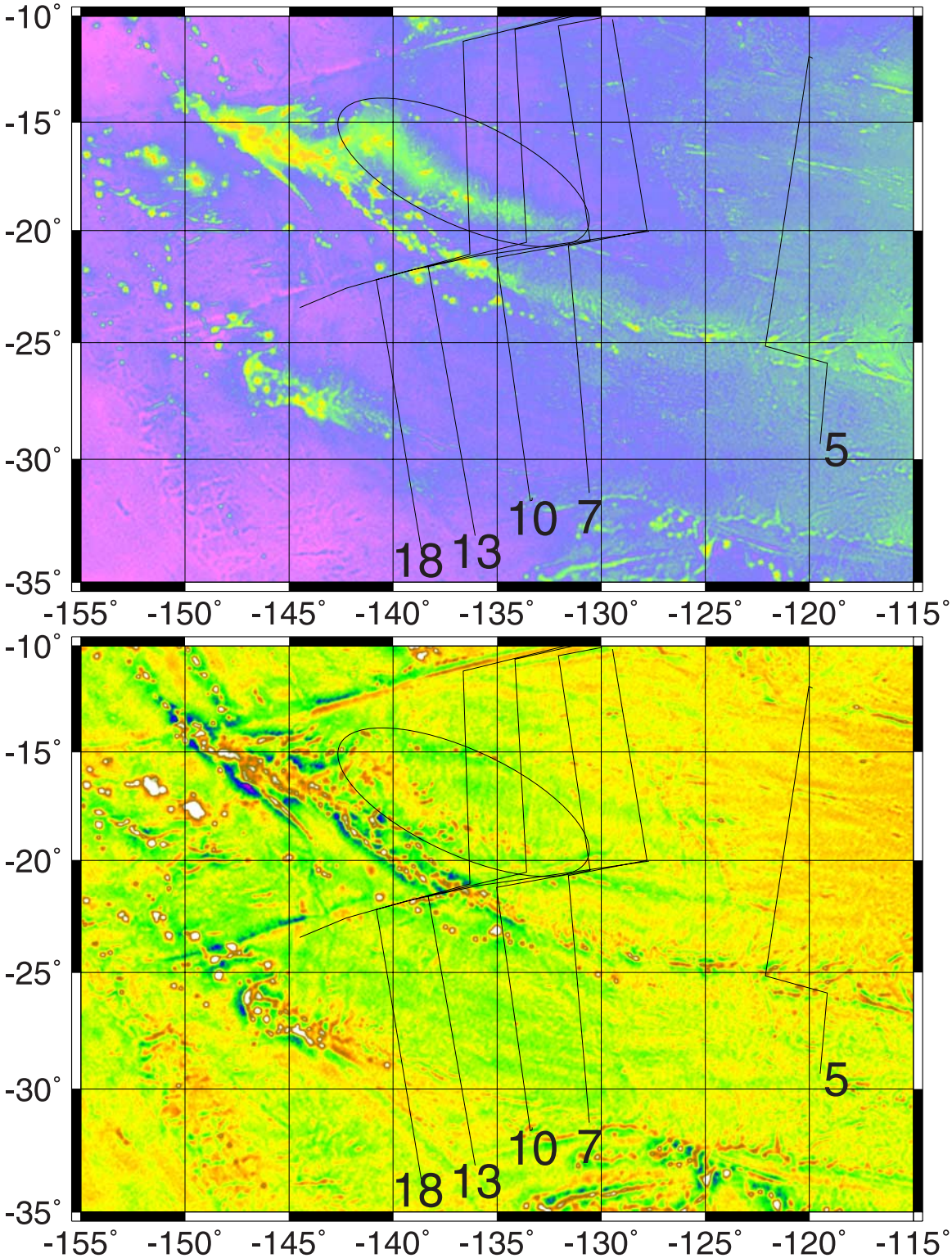


**Figure 14.** (top) South Pacific topography from the GTOPO30 data set [*Smith and Sandwell*, 1997]. (bottom) South Pacific gravity from *Sandwell and Smith* [1997]. Color scale is the same as in Figures 11 and 13. Magnetic anomalies are from *Mayes et al.* [1990]. The eastern Tuamotu Island Plateau is circled.

[46] Since this paper uses a rather detailed plate reconstruction, it now also makes sense to discuss some of the detailed features of the computed hot spot motion, compare them to observations, and devise a scenario that can explain the observations and is in accord with the results shown here.

[47] In this comparison, the Easter hot spot track is regarded to run roughly along the grey line (Sala y Gomez Ridge Main trend) shown in Figure 12. Particularly in the gravity map (Figure 13), this appears as the clearest linear feature. It also marks the south-eastern boundary of anomalous sea floor features. Other topographic and gravity features between the Nazca fracture zone and this line may be caused by interaction of the plume with the spreading ridge and/or the transform fault/fracture zone. Some of these features have the form of elongated ridges - two of the clearest examples are outlined in Figure 12, and similar features in the Musicians seamounts have been interpreted to represent plume-ridge interaction [*Phipps Morgan et al.*, 2000]. Such an interpretation implies that the plume interacted with the ridge and/or fracture zone/transform fault over a distance of at least ~300 km (distance between points B and E in Figure 12).

[48] Symmetric spreading, which is assumed here, introduces ridge jumps in the plate reconstruction that are not necessarily real. However, there are features visible on the topographic and gravity maps (Figures 11 and 13), and schematically drawn in Figure 12, that are evidence for a least two ridge jumps occurring north of the Sala y Gomez ridge: The north-south trending topographic ridge at ≈94°W may be an extinct spreading ridge, and possible escarpments to the east and west of it may mark the locations where new spreading started, as escarpments are typical features that result when a new spreading center intrudes older ocean floor [*Marquart*, 1997]. The features can thus be explained by a first ridge jump equal to or smaller than the distance between chron 7 and the eastern escarpment, i.e. of a few hundred km, that occurred after chron 7 (≈25 Ma). The spreading along this new ridge would then have continued for a few Ma, corresponding to the distance between the fossil spreading ridge and the escarpments, before the ridge jumped yet another few hundred km to the west, leaving both escarpments and the (now fossil) ridge on the Nazca plate. Thus, timing, magnitude and locations of the ridge jumps assumed in this paper are approximately in accord with the interpretation of these features given by *Marquart* [1997].

[49] For each ridge jump, an eastward "kink" of hot spot motion is computed (e.g., Figure 4), rather similar in shape and size to a kink in what is regarded as the actual hot spot track – the part of the grey line between points B and C in Figure 12. However, if the hot spot motion is combined with the fast Nazca plate motion, there is no kink in the computed hot spot track (Figures 12 and 13), and in order to maintain such a kink in the hot spot track, it would be necessary that the Nazca plate slowed down dramatically after the spreading along the old ridge ceased and before it again reached a high rate along the new ridge. As the kink in the computed hot spot motion is caused by a slowing of the return flow towards the ridge at the plume location, there would be an even larger kink with such a modified plate motion history. However, such a temporary slowdown in plate motion is not supported by other evidence.

[50] Based on one radiometrically dated sample in that region [*O'Connor et al.*, 1995], seamounts at the northern end of the kink (point B in Figure 12) should have formed at ≈25 Ma, corresponding to the time of chron 7, and the first ridge jump in the plate reconstruction used. This would imply, that at this time, before the ridge jump occurred, the hot spot was located ≈300 km east of the eastern intersection of ridge and Nazca Fracture Zone, which is clearly within the range of the computations shown in Figures 4 to 10. All the computations shown in Figures 4–7 imply that the distance between ridge and hot spot has either decreased or stayed similar between chron 13 (≈33 Ma) and chron 7 (≈25 Ma). This would therefore mean that the age at point A in Figure 12 should correspond to younger than chron 10 (≈28.3 Ma).

[51] Whereas the Sala y Gomez ridge and the presumed hot spot track south of the Nazca fracture zone consist of isolated seamounts which are

clearly visible on both topographic and gravity maps (Figures 11 and 13), the Nazca ridge north of the Nazca fracture zone is broader and smoother and is almost invisible on the gravity map. This different morphology suggests a different origin: The isolated seamounts south of the fracture zone and farther west may have formed directly above the plume, in an intraplate location: a seamount that is built on already cooled and thickened lithosphere will not be isostatically compensated. It will thus be associated with a gravity high. It will also depress the surrounding lithosphere and thus be surrounded by a gravity low, in agreement with observations (Figure 13). The Nazca ridge north of the Nazca fracture zone may in contrast have formed on the spreading ridge. This would allow better isostatic compensation, and explain why it is almost invisible on the gravity map. Formation of the Nazca ridge on the spreading ridge is also supported by the observation that the eastern part of the Tuamotu Island Plateau in relation to the isochrons (Figure 14) is almost the mirror image of the Nazca ridge (Figure 11). It is also, in its broad outline, almost invisible on the gravity map. A near-ridge origin of the Tuamotu plateau is also in agreement with other observations [*Ito and McNutt*, 1993].

[52] Based on the computations performed, and the observations just discussed, the following scenario is proposed: Off-ridge volcanic activity directly above the Easter plume began only once the plume was south of the Nazca fracture zone, forming the seamount at point A in Figure 13, less than ≈28.3 Ma. Since the Nazca plate had a northward component of motion, the plume was north of the fracture zone before that, and all material erupted at the ridge. However, between ≈43 and 28.3 Ma, the plume was several hundred km east of the ridge (see also Figures 4–7). The southwestern end of the Nazca ridge is a broad volcanic feature formed at about chron 10 (point D in Figure 12). This marks the transition from on-ridge to intraplate volcanism, at about the same time as, or slightly before formation of the first isolated seamounts (point A in Figure 13).

[53] During the time of isolated seamount formation, the elongated ridges (Figure 12) between the presumed hot spot track and the fracture zone are evidence for continued interaction between the plume and the system spreading ridge/transform fault/fracture zone. Plume-ridge interaction over distances of several hundred km should be possible also according to a variety of geophysical and geochemical evidence as well as numerical models [*Ribe*, 1996; *Ito and Lin*, 1995]. It is however not evident why the plume-ridge interaction would have changed in character once the plume was south of the fracture zone, and hence located beneath older lithosphere. Assuming a fixed hot spot, in which case the plume is located much closer to the ridge during the time interval 43–25 Ma (Figure 11) offers an easier explanation for the formation of Nazca ridge and the the eastern part of the Tuamotu Island Plateau, but it does not explain the age data as well as computations that include hot spot motion.

[54] The fact that any model that fits available age data on the Sala y Gomez ridge well predicts a plume location several hundred km to the East of the ridge during formation of the Nazca ridge is merely a result of the fact that the extrapolation of the best-fitting line through the available age dates (dots in Figures 11–13, upper panels) is offset by several hundred km from the line through the isochron ages (shown as crosses in these figures). Assuming the observations and models adopted here (age data, anomaly picks, plate reconstructions etc.) are more or less correct, this prediction could only be avoided with an eastward hot spot motion of a few hundred km during a few Ma, however any episodes of eastward hot spot motion that occur in the computations (e.g. Figure 4) amount to much less than that. This prediction contrasts with known present-day examples of hot spots that do lie off-ridge and influence ridge melting, but whose greatest volcanic output is directly over the hot spot (e.g., Galapagos).

[55] Clearly the new age data from Drift Expedition Leg 6 will help to assess which models of hot spot motion (or fixity) are most realistic, and will allow a much better evaluation of how realistic the scenario proposed here, and the numerical model used is.

[56] In order to better understand formation of features possibly caused by plume-ridge interac-

tion, it will be necessary to apply other numerical techniques than the one used here. Particularly, if new data corroborate the conclusion of a hot spot located off-ridge that did not produce any volcanic trail directly above the hot spot, then further numerical models that include the dynamics of melting and melt migration would be warranted to study the question whether such a scenario can be reproduced using realistic input parameters.

[57] This paper is primarily concerned with the past 43 Ma, because "absolute" Pacific plate motion prior to that is more controversial, and hence there is considerable additional uncertainty. Nevertheless a few remarks about older features possibly related to the Easter hot spot are appropriate, since an initiation age 60–120 Ma is modeled. As discussed above, for a hot spot location at Easter Island, older ages than observed are predicted in the Line Islands, even if hot spots are assumed fixed. If hot spot motion is considered, this misfit increases. It is therefore suggested that Line Islands were not formed by the Easter hot spot either, but possibly a hot spot located beneath the Pacific plate and roughly moving coherently with the Hawaii and Louisville hot spots. The Easter hot spot may not have left any track on the Pacific plate prior to the formation of the eastern part of the Tuamotu Island platform (which is circled in Figure 14 and, if formed at the ridge, started forming around 60 Ma ago, based on the isochrons), simply because it was located beneath the Nazca or Farallon plate and far enough away from the spreading ridge that it didn't interact. The location of the plume relative to the ridge prior to 43 Ma ago is less clear, because the Pacific absolute plate motion is controversial. According to one scenario [*Tarduno and Cottrell*, 1997] the Emperor trend represents motion of the Hawaiian hot spot, whereas the Pacific plate would have moved only little during its formation (≈80–43 Ma). If its motion was slower than the half-spreading rate between Pacific and Nazca or Farallon plate during that time, the ridge would presumably have moved eastward and would have been farther away from the Easter hot spot earlier. The interpretation of new paleomagnetic data [*Tarduno et al.*, 2001] will also put better constraints on that earlier time period.

## Acknowledgments

[58] Bob Duncan provided valuable information and motivation for this work. I also thank Peter Molnar for comments on the manuscript, Gabriele Marquart for discussions, Michael Manga and Ben-Yuan Kuo for comments on an older version of the manuscript, Rick O'Connell for continuing encouragement to pursue this work, all the authors of the tomography models for making their models publicly available, David Naar for supplying unpublished age data, and Geoff Davies and Robert Duncan for two insightful reviews as well as guest editor David Graham for a number of further suggestions. Figures were prepared using GMT graphics [*Wessel and Smith*, 1995].

## References

Berggren, W. A., D. V. Kent, C. C. Swisher, and M.-P. Aubry, A revised Cenozoic geochronology and chronostratigraphy, in *Geochronology, Time Scales and Global Stratigraphic Correlation*, Spec. Publ. 54, edited by W. A. Berggren et al., pp. 129–212, SEPM, Tulsa, Okla., 1995.

Bijwaard, H., W. Spakman, and E. R. Engdahl, Closing the gap between regional and global travel time tomography, *J. Geophys. Res.*, *103*, 30,055–30,078, 1998.

Bonatti, E., C. G. A. Harrison, D. E. Fisher, J. Honnorez, J.-G. Schilling, J. J. Stipp, and M. Zentilli, Easter volcanic chain (Southeast Pacific): A mantle hot line, *J. Geophys. Res.*, *82*, 2457–2478, 1977.

Cande, S. C., C. A. Raymond, J. Stock, and W. F. Haxby, Geophysics of the Pitman Fracture Zone and Pacific-Antarctic plate motions during the Cenozoic, *Science*, *270*, 947–953, 1995.

Cande, S. C., J. M. Stock, and T. Ishihara, Cenozoic motion between East and West Antarctica, *Nature*, *404*, 145–150, 2000.

Chang, T., J. Stock, and P. Molnar, The rotation group in plate tectonics and the representation of uncertainties of plate reconstructions, *Geophys. J. Int.*, *101*, 649–661, 1990.

Clague, D. A., and G. B. Dalrymple, Tectonics, geochronology, and origin of the Hawaiian-Emperor volcanic chain, in *The Geology of North America, Volume N, The Eastern Pacific Ocean and Hawaii*, edited by E. L. Winterer, D. M. Hussong, and R. W. Decker, pp. 188–217, Geol. Soc. of Am., Boulder, Colo., 1989.

Davies, G. F., Ocean bathymetry and mantle convection, 1, Large-scale flow and hot spots, *J. Geophys. Res.*, *93*, 10,467–10,480, 1988.

Davies, G. F., Temporal variation of the Hawaiian plume flux, *Earth Planet. Sci. Lett.*, *113*, 277–286, 1992.

Duncan, R. A., and D. A. Clague, Pacific plate motion recorded by linear volcanic chains, in *The Ocean Basins and Margins*, vol. 7a, edited by A. E. M. Nairn, F. G. Stehli, and S. Uyeda, pp. 89–121, Plenum, New York, 1985.

Gordon, R. G., and D. Jurdy, Cenocoic global plate motions, *J. Geophys. Res.*, *91*, 12,389–12,406, 1986.

Grand, S. P., Mantle shear structure beneath the Americas and surrounding Oceans, *J. Geophys. Res.*, *99*, 11,591–11,621, 1994.

Grand, S. P., R. D. Van der Hilst, and S. Widiyantoro, Global seismic tomography: A snapshot of convection in the Earth, *GSA Today*, *7*, 1–7, 1997.

Griffiths, R. W., and I. H. Campbell, Stirring and structure in mantle plumes, *Earth Planet. Sci. Lett.*, *99*, 66–78, 1990.

Haase, K. M., C. W. Devey, and S. L. Goldstein, Two-way exchange between the Easter mantle plume and the Easter microplate spreading axis, *Nature*, *382*, 344–346, 1996.

Hager, B. H., and R. J. O'Connell, Kinematic models of large-scale flow in the Earth's mantle, *J. Geophys. Res.*, *84*, 1031–1048, 1979.

Hager, B. H., and R. J. O'Connell, A simple global model of plate dynamics and mantle convection, *J. Geophys. Res.*, *86*, 4843–4867, 1981.

Hanan, B. B., and J.-G. Schilling, Easter microplate evolution: Pb isotope evidence, *J. Geophys. Res.*, *94*, 7432–7448, 1989.

Ito, G., and J. Lin, Oceanic spreading center-hot spot interactions: Constraints from along-isochron bathymetric and gravity anomalies, *Geology*, *23*, 657–660, 1995.

Ito, G., and M. McNutt, Volcanic structure of the Tuamotu island plateau from multi-channel and refraction seismics: Evidence for a near ridge origin, International Workshop on the Polynesian Plume Province, Papeete, Tahiti, 1993.

Keller, R. A., R. A. Duncan, and M. R. Fisk, Geochemistry and $^{40}Ar/^{39}Ar$ geochronology of basalts from ODP Leg 145, *Proc. Ocean Drill. Prog., Sci. Results*, *145*, 333–344, 1995.

Kingsley, R. H., and J.-G. Schilling, Plume-ridge interaction in the Easter-Sala y Gomez seamount chain-Easter microplate system: Pb isotope evidence, *J. Geophys. Res.*, *103*, 24,159–24,177, 1998.

Lithgow-Bertelloni, C., M. A. Richards, Y. Ricard, R. J. O'Connell, and D. C. Engebretson, Toroidal-poloidal partitioning of plate motions since 120 Ma, *Geophys. Res. Lett.*, *20*, 375–378, 1993.

Marquart, G., Satellite derived gravity of the Nazca plate - implications for tectonic reconstructions and age structure (abstract), *Terra Nova*, *9*(suppl.), 314, 1997.

Masters, G., G. Laske, H. Bolton, and A. Dziewonski, The relative behavior of shear velocity, bulk sound speed, and compressional velocity in the mantle: implications for chemical and thermal structure, in *Seismology and Mineral Physics, Geophys. Monogr. Ser.*, vol. 117, edited by S. Karato, pp. 63–87, AGU, Washington, D.C., 2000.

Mayes, C. L., L. A. Lawver, and D. T. Sandwell, Tectonic history and new isochron chart of the South Pacific, *J. Geophys. Res.*, *95*, 8543–8567, 1990.

Mégnin, C., and B. Romanowicz, The shear velocity structure of the mantle from the inversion of of body, surface and higher modes waveforms, *Geophys. J. Int.*, *143*, 709–728, 2000.

Molnar, P., and J. Stock, Relative motions of hot spots in the Pacific, Atlantic and Indian Ocean since late Cretaceous time, *Nature*, *327*, 587–591, 1987.

Morgan, W. J., Deep mantle convection plumes and plate motions, *Am. Assoc. Pet. Geol. Bull.*, *56*, 203–213, 1972.

Müller, R. D., W. R. Roest, J.-Y. Royer, L. M. Gahagan, and J. G. Sclater, Digital isochrons of the world's ocean floor, *J. Geophys. Res.*, *102*, 3211–3214, 1997.

Müller, R. D., W. R. Roest, and J.-Y. Royer, Asymmetric sea-floor spreading caused by ridge-plume interactions, *Nature*, *396*, 455–459, 1998.

O'Connell, R. J., C. W. Gable, and B. H. Hager, Toroidal-poloidal partitioning of lithospheric plate motions, in *Glacial Isostasy, Sea Level and Mantle Rheology*, edited by R. Sabadini and K. Lambeck, pp. 535–551, Kluwer Acad., Norwell, Mass., 1991.

O'Connor, J. M., P. Stoffers, and M. O. McWilliams, Time-space mapping of Easter Chain volcanism, *Earth Planet. Sci. Lett.*, *136*, 197–212, 1995.

Olson, P., and H. Singer, Creeping plumes, *J. Fluid Mech*, *158*, 511–531, 1985.

Pan, Y., and R. Batiza, Major element chemistry of volcanic glasses from the Easter Seamount Chain: Constraints on melting conditions in the plume channel, *J. Geophys. Res.*, *103*, 5287–5304, 1998.

Pardo-Casas, F., and P. Molnar, Relative motion of the Nazca (Farallon) and South American plates since late Cretaceous time, *Tectonics*, *6*, 233–248, 1987.

Phipps Morgan, J., et al., Morphology and structure of two 400 km-long volcanic ridges in the Musicians Seamount province, European Geophysical Society Meeting, Eur. Geophys. Soc., Nice, France, 2000.

Raymond, C. A., J. M. Stock, and S. C. Cande, Fast Paleogene motion of the Pacific hot spots from revised global plate circuit constraints, in *The History and Dynamics of Global Plate Motions*, Geophys. Mon. Ser., vol. 121, edited by M. A. Richards, R. G. Gordon, and R. D. van der Hilst, pp. 359–375, AGU, Washington, DC, 2000.

Ribe, N. M., The dynamics of plume-ridge interaction, 2, Off-ridge plumes, *J. Geophys. Res.*, *101*, 16,195–16,204, 1996.

Ribe, N. M., and U. R. Christensen, The dynamical origin of Hawaiian volcanism, *Earth Planet. Sci. Lett.*, *171*, 517–531, 1999.

Richards, M. A., Hot spots and the case for a high viscosity lower mantle, in *Glacial Isostasy, Sea Level and Mantle Rheology, NATO ASI Ser. C*, vol. 334, edited by R. Sabadini, K. Lambeck, and E. Boschi, pp. 571–587, Kluwer Acad., Norwell, Mass., 1991.

Richards, M. A., and R. W. Griffiths, Deflection of plumes by mantle shear flow: Experimental results and a simple theory, *Geophys. J.*, *94*, 367–376, 1988.

Richards, M. A., R. A. Duncan, and V. E. Courtillot, Flood basalts and hot spot tracks: Plume heads and tails, *Science*, *246*, 103–107, 1989.

Ritsema, J., and H. J. Van Heijst, Seismic imaging of structural heterogeneity in Earth's mantle: Evidence for large-scale mantle flow, *Sci. Prog.*, *83*, 243–259, 2000.

Sandwell, D. T., and W. H. F. Smith, Marine gravity anomaly from Geosat and ERS 1 satellite altimetry, *J. Geophys. Res.*, *102*, 10,039–10,054, 1997.

Schilling, J.-G., Fluxes and excess temperatures of mantle plumes inferred from their interaction with migrating mid-ocean ridges, *Nature*, *352*, 397–403, 1991.

Sleep, N., Hot spots and mantle plumes: Some phenomenology, *J. Geophys. Res.*, *95*, 6715–6736, 1990.

Smith, W. H. F., and D. T. Sandwell, Global seafloor topogra-

phy from satellite altimetry and ship depth soundings, *Science*, *277*, 1957–1962, 1997.

Steinberger, B., Plumes in a convecting mantle: Models and observations for individual hotspots, *J. Geophys. Res.*, *105*, 11,127–11,152, 2000.

Steinberger, B. M., and A. R. Calderwood, Mineral physics constraints on viscous flow models of mantle flow, *J. Conf. Abs.*, *6*, 423–424, 2001.

Steinberger, B., and R. J. O'Connell, Advection of plumes in mantle flow: Implications for hot spot motion, mantle viscosity and plume distribution, *Geophys. J. Int.*, *132*, 412–434, 1998.

Steinberger, B., and R. J. O'Connell, Effects of mantle flow on hot spot motion, in *The History and Dynamics of Global Plate Motions, Geophys. Monogr. Ser.*, vol. 121, edited by M. A. Richards, R. G. Gordon, and R. D. van der Hilst, pp. 377–398, AGU, Washington, D.C., 2000.

Su, W.-J., R. L. Woodward, and A. M. Dziewonski, Degree 12 model of shear velocity heterogeneity in the mantle, *J. Geophys. Res.*, *99*, 6945–6980, 1994.

Tarduno, J. A., and R. D. Cottrell, Paleomagnetic evidence for motion of the Hawaiian hot spot during formation of the Emperor seamounts, *Earth Planet. Sci. Lett.*, *153*, 171–180, 1997.

Tarduno, J. A., R. A. Duncan, R. D. Cottrell, and D. W. Scholl, Motion of Hawaiian hot spot during formation of the emperor seamounts: Initial results of ODP Leg 197, *Eos Trans. AGU*, *82*(47), Fall Meet. Suppl., F1116, 2001.

Tebbens, S. F., and S. C. Cande, Southeast Pacific tectonic evolution from the early Oligocene to Present, *J. Geophys. Res.*, *102*, 12,061–12,084, 1997.

Watts, A. B., J. K. Weissel, R. A. Duncan, and R. L. Larson, Origin of the Louisville Ridge and its relationship to the Eltanin Fracture Zone System, *J. Geophys. Res.*, *93*, 3051–3077, 1988.

Wessel, P., and L. W. Kroenke, A geometric technique for relocating hot spots and refining absolute plate motions, *Nature*, *387*, 365–369, 1997.

Wessel, P., and W. H. F. Smith, New version of the Generic Mapping Tools released, *Eos Trans. AGU*, *76*(29), 329, 1995.

Whitehead, J. A., and D. S. Luther, Dynamics of laboratory diapir and plume models, *J. Geophys. Res.*, *80*, 705–717, 1975.